

KUNGLIGA TEKNISKA HÖGSKOLAN

Department of Chemistry

Division of Applied Physical Chemistry - Nuclear Chemistry

Master Thesis

Impact of Peroxide Speciation on the Kinetics
of Oxidative Dissolution of UO_2

Hazal Aydogan

Supervisor: Prof. Mats Jonsson



Stockholm Sweden, Spring 2022

Abstract

Disposal of spent nuclear fuels is of great importance to prevent the environment and humans from being affected by long-lived radionuclides for 100,000 years or more. Even though the deep geological repositories are designed to remain durable for many years, spent nuclear fuel may come in contact with groundwater in case of a multi-barrier failure. The inherent radioactivity of spent nuclear fuel causes water radiolysis producing oxidizing and reducing agents. Among the radiolysis products, hydrogen peroxide (H_2O_2) is reported as a primary contributor to the oxidative dissolution of the fuel matrix, UO_2 . Although UO_2 has low solubility in water, oxidized UO_2 , UO_2^{2+} , has several orders of magnitude higher solubility. This poses the risk of the radionuclides being released into the environment. Bicarbonate (HCO_3^-) is one of the main components of groundwater and is known to increase the dissolution of UO_2^{2+} . Therefore, in this study, the effects of HCO_3^- concentration on the oxidative dissolution of UO_2 were investigated by keeping the initial amount of H_2O_2 constant at 0.2 mM and changing the HCO_3^- concentration (1 mM, 2 mM, 5 mM, and 10 mM). Besides, the effect of UO_2^{2+} on the speciation was investigated by adding uranyl nitrate ($\text{UO}_2(\text{NO}_3)_2 \times 6\text{H}_2\text{O}$) to the systems before exposure to H_2O_2 . The impact of speciation on the kinetics of oxidative dissolution of UO_2 was analyzed. As a result of experiments, it has been concluded that the amount of dissolved UO_2^{2+} is higher in higher HCO_3^- concentration. Also, the rate of the UO_2^{2+} dissolution decreases with addition of UO_2^{2+} due to the complexes formed in the systems. It was observed that oxidation of UO_2 is the rate limiting reaction at the beginning of the exposure; therefore there is a delay in the UO_2^{2+} dissolution. On the other hand, it has been seen that the HCO_3^- deficiency limits the dissolution capacity of the systems. Free H_2O_2 is the dominant peroxide species in the systems without initially added UO_2^{2+} , while -6 and -2 charged complexes are dominant in the systems with initially added UO_2^{2+} . The H_2O_2 complexes are found more effective on the surface mechanism in the systems having lower HCO_3^- concentration. There is no observable trend in H_2O_2 consumption rate with respect to HCO_3^- concentration. Therefore, it was concluded that the H_2O_2 consumption rate is independent of dissolution reaction. Finally, the dissolution in the system without initially added UO_2^{2+} follows the first-order kinetics with respect to HCO_3^- concentration.

Contents

Abstract	iii
1 Introduction	1
1.1 Aim of the study	1
2 Theory	3
2.1 Nuclear Fuels	3
2.1.1 Spent Nuclear Fuel	3
2.2 Nuclear Waste Disposal	4
2.3 Oxidative Dissolution of UO ₂	4
2.3.1 Radiolysis of Water	5
2.3.2 Effect of Bicarbonate	6
2.3.3 Effect of Ionic Strength	8
3 Materials and Method	9
3.1 Materials	9
3.1.1 UO ₂ Powder	9
3.1.2 Instrumentation and Software	9
3.2 Methodology	10
3.2.1 Ghormley Triiodide Method	10
3.2.2 Arsenazo III Method	10
4 Experimental Procedure	11
4.1 Washing of powder	11
4.2 Preparation of stock solutions and reagents	11
4.3 UO ₂ powder exposure	12
5 Results and Discussion	14
5.1 Oxidative Dissolution of UO ₂	14
5.2 Long-Term Oxidative Dissolution of UO ₂	22
5.3 Oxidative Dissolution Effect on pH	23
5.4 Speciation Calculation	25

5.5 Kinetic Analysis	30
6 Conclusion	37
Acknowledgments	38
References	44
Appendix	45

List of Figures

2.1	HCO_3^- concentration at different depths in groundwater	7
5.1	UO_2^{2+} concentration as a function of time in the systems that have 0.2 mM H_2O_2 , and 10 mM, 5 mM, 2 mM, and 1 mM HCO_3^- (a) without initially added UO_2^{2+} (b) with initially added 0.3 mM UO_2^{2+}	15
5.2	UO_2^{2+} and the peroxide concentrations as a function of time in the systems; (a) 10 mM HCO_3^- , (b) 5 mM HCO_3^- , (c) 2 mM HCO_3^- , (d) 1 mM HCO_3^- with 0.2 mM H_2O_2 and without initially added UO_2^{2+}	17
5.3	The UO_2^{2+} concentration (the concentration at time t subtracted from the initial concentration) and the peroxide concentration as a function of time in the systems with initially added UO_2^{2+} , 0.2 mM H_2O_2 ; (a) 10 mM HCO_3^- , (b) 5 mM HCO_3^- , (c) 2 mM HCO_3^- , (d) 1 mM HCO_3^-	19
5.4	UO_2^{2+} concentration as a function of time in the systems that have 0.2 mM H_2O_2 , and 10 mM, 5 mM, 2 mM and 1 mM HCO_3^- with and without initially added 0.3 mM UO_2^{2+}	21
5.5	Concentrations of (a) H_2O_2 , (b) UO_2^{2+} as a function of time for the systems have 0.2 mM H_2O_2 , and 10 mM, 5 mM, 2 mM, and 1 mM HCO_3^- , with initially added 0.3 mM UO_2^{2+} ; and 2 mM and 1 mM HCO_3^- , 0.2 mM H_2O_2 without initially added UO_2^{2+}	22
5.6	Speciation calculation prepared in SPANA with the data at (a) 0.5 min, (b) 60 min and (c) 300 min of exposure for the system with 5 mM HCO_3^- , 0.2 mM H_2O_2 with initially added 0.3 mM UO_2^{2+}	24
5.7	Concentration of the H_2O_2 species calculated from SPANA as a function of time for the systems that have 0.2 mM H_2O_2 , and (a) 10 mM HCO_3^- , (b) 5 mM HCO_3^- , (c) 2 mM HCO_3^- (d) 1 mM HCO_3^- without initially added UO_2^{2+}	26
5.8	Concentration of the H_2O_2 species calculated from SPANA as a function of time for the systems that have 0.2 mM H_2O_2 , and (a) 10 mM HCO_3^- , (b) 5 mM HCO_3^- , (c) 2 mM HCO_3^- (d) 1 mM HCO_3^- with initially added 0.3 mM UO_2^{2+}	28

5.9	The H_2O_2 consumption in the first 15 min of exposure and its multi-exponential fit as a function of time for the systems with different HCO_3^- concentrations and without initially added UO_2^{2+}	31
5.10	Natural logarithm of H_2O_2 consumption in the first 15 min of exposure as a function of time for the systems with different HCO_3^- concentrations and without initially added UO_2^{2+}	32
5.11	The H_2O_2 consumption in the first 15 min of exposure and its multi-exponential fit as a function of time for the systems with different HCO_3^- concentrations and with initially added 0.3 mM UO_2^{2+}	34
5.12	The UO_2^{2+} concentration in the first 15 min of exposure and its multi-exponential fit as a function of time for the systems with different HCO_3^- concentrations and without initially added UO_2^{2+}	35
5.13	The UO_2^{2+} concentration in the first 15 min of exposure and its multi-exponential fit as a function of time for the systems with different HCO_3^- concentrations and with initially added 0.3 mM UO_2^{2+}	36

List of Tables

4.1	Experimental conditions.	13
5.1	HCO ₃ ⁻ speciation calculated from SPANA as a fraction of HCO ₃ ⁻ for the systems that have 10 mM, 5 mM, 2 mM and 1 mM HCO ₃ ⁻ , 0.2 mM H ₂ O ₂ with and without initially added 0.3 mM UO ₂ ²⁺ at 300 min of exposure.	30
5.2	Free H ₂ O ₂ concentration determined from SPANA for time = 0.5 min, the rate, the first-order and the second order rate constants for the systems with 0.2 mM H ₂ O ₂ , different HCO ₃ ⁻ concentrations without initially added UO ₂ ²⁺	33

Chapter 1

Introduction

The disposal of spent nuclear fuels constitutes the final step of the nuclear fuel cycle. Spent nuclear fuels contain long-lived radionuclides. Therefore, spent fuel must be stored so that the environment and humans are protected from the harm of the radionuclides for hundreds of thousands of years. The multi-barrier concept is proposed as a method for final geological disposal. In case of a multi-barrier failure, radionuclides may be released into the environment [1].

Knowing the factors that may cause radionuclides to reach the environment or humans and the mechanisms of these processes after possible multi-barrier failures under deep geological repository conditions is essential.

One of the main subjects mostly studied is the oxidative dissolution of spent nuclear fuel. Some factors that affect the oxidative dissolution mechanism are oxidizing and reducing agents [2, 3, 4, 5], hydrogen peroxide (H_2O_2) [2, 6, 7, 8, 9, 10, 11, 12, 13, 14], bicarbonate (HCO_3^-) [2, 10, 15, 16, 17], complex formation [2, 7, 10, 11, 13, 17, 18, 19, 20, 21, 22, 23], pH [2, 12, 24], ratio between the surface area of solid and solution volume [9, 15, 24], irradiation [2, 14, 17, 25], ionic strength [12, 26, 27], and temperature [2, 23]. Since uranium dioxide (UO_2) constitutes the majority of spent nuclear fuel [15], UO_2 is often used to mimic the dissolution mechanism of spent nuclear fuel.

1.1 Aim of the study

The behavior of spent nuclear fuels under deep repository conditions in the presence of HCO_3^- and H_2O_2 has been studied by many researchers.

This study aimed to investigate the effect of HCO_3^- concentrations (1 mM, 2 mM, 5 mM, and 10 mM) on the oxidative dissolution of UO_2 in the presence of initial 0.2 mM H_2O_2 . The impact of H_2O_2 species on the oxidative dissolution kinetics of UO_2 was also aimed to be determined by initially adding 0.3 mM UO_2^{2+} .

According to the studies published on this subject, the following was hypothesized in this study: $\text{HCO}_3^-/\text{CO}_3^{2-}$ accelerate the UO_2^{2+} dissolution from the UO_2 surface; H_2O_2 consumption rate and UO_2^{2+} dissolution rate are reduced with initially added UO_2^{2+} and increase with increasing HCO_3^- concentration; H_2O_2 complexes are more effective on the surface mechanism in the systems having lower HCO_3^- concentration.

Chapter 2

Theory

2.1 Nuclear Fuels

Nuclear fuels are materials used to produce heat from a fission reaction. In general, nuclear fission is a reaction where the nucleus splits into smaller nuclei releasing a large amount of heat. Even though the heavy and unstable isotopes can be fissioned spontaneously by decaying, fission reactions occur also when fissile materials are bombarded with a neutron that is released in a prior fission event in nuclear reactors. These fissile elements are ^{233}U , ^{235}U , and ^{239}U . A similar reaction can occur with a fissionable elements such as ^{238}U with fast neutrons that provide high energy [28]. Uranium can be used as natural or slightly-enriched as in CANDU reactors or as enriched as in LWRs.

There are several types of nuclear fuels, including oxides, carbides, nitrides, and silicides [29]. UO_2 is the most common nuclear fuel for conventional reactors and can be used directly or as a mixture with PuO_2 , which is termed mixed oxide (MOX) fuel. UO_2 is preferred as a fuel because of its thermal stability and good compatibility with other materials used in nuclear reactors, such as coolant and cladding [30].

2.1.1 Spent Nuclear Fuel

Spent nuclear fuel is generated during the operation of nuclear power reactors, including research reactors, isotope production reactors, and propulsion reactors. Since UO_2 composes the majority of the nuclear fuels, spent nuclear fuel mainly consists of UO_2 [31].

Spent nuclear fuels can no longer sustain nuclear reaction in typical thermal reactors due to depletion of fissile materials and buildup of fission products. Therefore, it must be replaced with fresh nuclear fuel regularly.

Spent nuclear fuel can be reprocessed or stored in deep geological repositories. Spent nuclear fuels mainly consist of uranium (94%), fission products (4-5%), plutonium (1%) and minor actinides (0.1%). Neptunium (Np), americium (Am), and curium (Cm), belonging to minor-actinides, are long-lived α -emitting radionuclides and must be stored for hundreds of thousands of years. Therefore, spent nuclear fuels are categorized as high-level nuclear waste and must be managed safely and effectively [32].

2.2 Nuclear Waste Disposal

If reprocessing is not considered in a nuclear fuel cycle, spent nuclear fuels must be kept isolated from the biosphere to protect the environment and humans against their harmful effects. Even though there are pools and interim storage to cool the spent nuclear fuel after fission, spent nuclear fuels must be stored until their radioactivity reaches the level of natural uranium. A deep geological repository is an accepted method to store spent nuclear fuels. The deep geological repositories must be stable for hundreds of thousands of years due to the long-lived α -emitters in spent nuclear fuels. These repositories are designed consisting of multi-barriers for the long-term stability of spent nuclear fuel [31, 33, 34].

Both Sweden and Finland work on the KBS-3 repository concept. In this concept, spent nuclear fuel is encapsulated in copper canisters to mitigate the dispersion of radionuclides and stay stable under possible mechanical and corrosion loads. These canisters are placed at a depth of 400-700 meters in crystalline bedrock. For mechanical protection and prevention of underground water flow in the deposition area, the canisters are surrounded by bentonite clay buffer. The cavities are back-filled and closed to prevent underground water flow through the tunnels and the openings and maintain multi-barrier functions [33, 35].

2.3 Oxidative Dissolution of UO_2

The geological disposal is designed to keep spent nuclear fuel inside the repository to mitigate their effects on human health and the environment. However, spent nuclear fuel may contact groundwater in case of a multi-barrier failure, allowing radionuclides to migrate from the repository to the biosphere.

Spent nuclear fuel comprises mainly UO_2 [32]. Therefore, experimental studies mostly include the oxidative dissolution of UO_2 .

The composition of groundwater is an important factor in the oxidative dissolution of UO_2 . The concentrations of the ions and their ability to form ionic complexes with spent nuclear fuel change the dissolution behavior under repository conditions [8, 16, 33, 36, 37]. The components in the groundwater and their effect on the dissolution process will be discussed in Section 2.3.2 and Section 2.3.3.

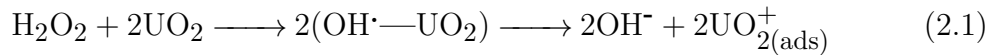
2.3.1 Radiolysis of Water

In contact between spent fuel and water, the inherent radioactivity of spent nuclear fuel causes water radiolysis. As a result of water radiolysis, some reactive oxidants ($\text{OH}\cdot$, HO_2 , H_2O_2) and reductants (e_{aq}^- , $\text{H}\cdot$, H_2) are formed [34, 38].

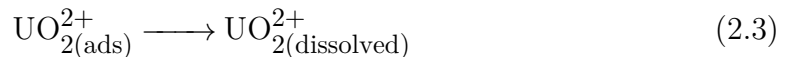
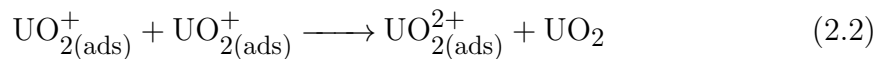
The chemical dissolution of UO_2 is negligible since UO_2 has low solubility, and the solubility limit of UO_2 is reached quickly under the conditions of a deep geological repository [33, 39]. It is also difficult to reduce UO_2 [40]. However, oxidants can easily change the reducing environment of groundwater and oxidize UO_2 to UO_2^{2+} . The solubility of UO_2^{2+} is higher than UO_2 [34, 41, 42, 43, 44]. Therefore, the dissolution rate of UO_2 increases with oxidation, and the release rate of radionuclides to the environment increases significantly.

Among the radiolysis products, H_2O_2 is considered the main component responsible for the oxidative dissolution of UO_2 . H_2O_2 may oxidize the UO_2 surface to UO_2^{2+} or undergo catalytic decomposition [2, 40].

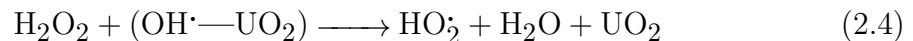
The proposed mechanism for the oxidation of UO_2 by H_2O_2 is given with Reaction 2.1, Reaction 2.2, and Reaction 2.3 [7, 27, 45].

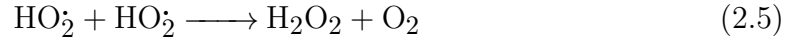


Uranium at oxidation state +V (UO_2^+) is further oxidized to UO_2^{2+} by an oxidant such as $\text{OH}\cdot$ and H_2O_2 or disproportionates to form UO_2^{2+} (oxidation state +VI) and UO_2 (oxidation state +IV) as given in Reaction 2.2. The final step is the dissolution of UO_2^{2+} from the UO_2 surface as given in Reaction 2.3 [15, 46].



On the other hand, catalytic decomposition of H_2O_2 on the UO_2 surface can be described as in Reaction 2.4 and Reaction 2.5 [7].





The oxidation of the UO_2 surface by H_2O_2 and catalytic decomposition of H_2O_2 on the UO_2 surface compete with each other [2, 45]. The intermediate product OH^\cdot , which is a surface-bound radical formed by adsorption of H_2O_2 on the UO_2 surface, is important because it can either oxidize the UO_2 surface as given in Reaction 2.1, or react with H_2O_2 as given in Reaction 2.4. The competition of these two mechanisms depends on the H_2O_2 concentration.

In the study conducted to analyze this competition, Fidalgo et al. (2018) [45] have shown that at low H_2O_2 concentration ($[\text{H}_2\text{O}_2] = 0.2 \text{ mM}$), the amount of H_2O_2 consumption and the UO_2^{2+} dissolution were similar. On the other hand, the amount of dissolved UO_2^{2+} per consumed H_2O_2 decreases with increasing initial H_2O_2 concentration.

Therefore, it has been concluded that the oxidation of UO_2 surface by H_2O_2 is dominant at H_2O_2 concentration of 0.2 mM and lower, while oxidation of UO_2 surface by H_2O_2 and catalytic decomposition of H_2O_2 on the UO_2 surface compete with each other at higher H_2O_2 concentrations [45].

2.3.2 Effect of Bicarbonate

Bicarbonate (HCO_3^-) is one of the main components of groundwater [47]. Frapce et al. (2004) [47] reported that there is a decreasing trend of HCO_3^- concentration with depth in nature. As illustrated in Figure 2.1 [47], the bicarbonate concentration is less than 100 mg.L^{-1} (approximately 1.6 mM) at a depth of 500 m which is the planned depth for geological repositories in Sweden and Finland [48]. It is also determined that the HCO_3^- concentration at 509 - 516 m depth is $1.8 \times 10^{-3} \text{ M}$ at $\text{pH} = 7.0$ [33].

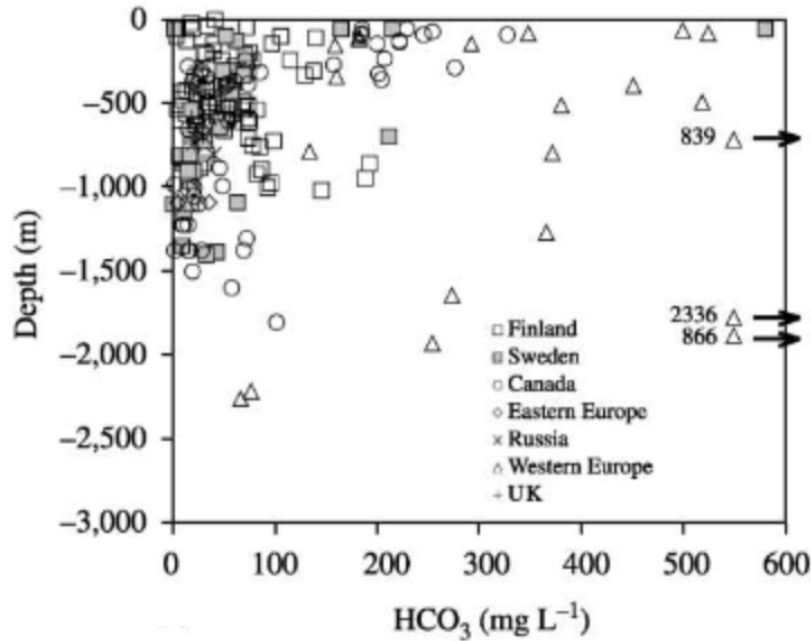


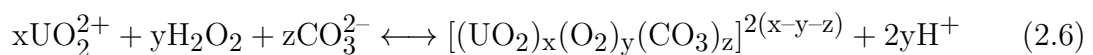
Figure 2.1: HCO_3^- concentration at different depths in groundwater

HCO_3^- is the main complexing agent in groundwater and enhances the dissolution of UO_2^{2+} (Reaction 2.3) from the oxidized UO_2 surface; therefore, the presence of HCO_3^- accelerates the dissolution process [15, 16, 27, 40].

For the HCO_3^- concentration above 1 mM, the rate constant for oxidation of UO_2 by H_2O_2 is shown as independent of HCO_3^- concentration, while the dissolution linearly increases with HCO_3^- for lower HCO_3^- concentrations (< 1 mM) in the presence of H_2O_2 [8, 16, 26]. Therefore, it has been concluded that the oxidation is the rate limiting step when HCO_3^- concentration is higher than 1 mM, while the dissolution is the rate limiting step for lower concentration of HCO_3^- [8]. Thus, oxidation of the spent fuel controls the dissolution of spent nuclear fuel under deep repository conditions (at around 1-2 mM HCO_3^-) [40].

Speciation Effect

UO_2^{2+} forms different complexes with HCO_3^- and H_2O_2 depending on the concentrations of UO_2^{2+} , H_2O_2 and HCO_3^- , and pH [7, 19, 49, 50]. The complex formation reaction is defined in Reaction 2.6 [10, 24].

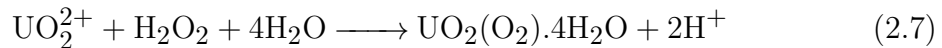


The H_2O_2 concentration has significant importance on the speciation in the uranyl-peroxide-carbonate system. A higher initial concentration of H_2O_2 causes the formation of uranyl-peroxide clusters which are highly soluble in water. The amount of H_2O_2 must be 10-20 times more than the uranium concentration to synthesize the clusters affecting the uranium speciation. On the other hand, smaller uranyl peroxide complexes are formed in the presence of lower concentration of H_2O_2 [11].

It was also reported that $\text{UO}_2(\text{O}_2)(\text{CO}_3)_2^{4-}$ is formed between pH 9 and 12. In the case of further increase of pH, the stability of $\text{UO}_2(\text{O}_2)(\text{CO}_3)_2^{4-}$ decreases, and it is converted to $\text{UO}_2(\text{CO}_3)_3^{4-}$ and $\text{UO}_2(\text{CO}_3)_x(\text{OH})_y^{2-2x-y}$ [21].

Studtite Formation

Studtite is a H_2O_2 mineral formed under certain conditions in the presence of H_2O_2 , UO_2^{2+} and HCO_3^- according to Reaction 2.7 [18, 51]:



Studtite formation is expected in no or low HCO_3^- concentration (< 1 mM) [8]. Studtite precipitates on the UO_2 surface and decreases the oxidation and dissolution rate of UO_2 because of its low solubility [13, 14]. Kim et al. (2018) reported that when HCO_3^- concentration decreases from 10 mM to 1 mM, the maximum amount of dissolved UO_2^{2+} decreases more than 10 times in alkali conditions (pH = 9) [18].

2.3.3 Effect of Ionic Strength

The dissolution behavior is affected by the surface charge of the UO_2 . The net charge of the UO_2 surface is equal to zero at a pH around 5, which is the Point of Zero Charge (PZC) [52]. When the pH of the medium is lower than PZC (pH < 5), the UO_2 surface becomes positively charged, resulting in the adsorption of the negatively charged ions on the surface. On the contrary, when the pH of the medium is higher than PZC (pH > 5), the UO_2 surface becomes negatively charged, and it causes repulsion between negatively charged ions and the surface.

Perchlorate (ClO_4^-) salts are used to investigate the ionic strength effect. It has been reported that 0.01 M and 0.1 M ClO_4^- has no significant effect on the PZC and the UO_2^{2+} dissolution [52]; however, it accelerates the H_2O_2 consumption [27]. ClO_4^- decreases the repulsion between equally charged surface by increasing ionic strength without changing the UO_2 dissolution mechanism. It was also reported that in the absence of HCO_3^- , the H_2O_2 consumption rate and UO_2^{2+} dissolution rate increase with ionic strength [27].

Chapter 3

Materials and Method

The chemicals used in the experiments were of reagent quality or higher purity. Before all measurements, the suspensions were filtered with 0.22 μm cellulose acetate syringe filters. However, in the experiments that lasted more than 3 days, the particles were observed in the filtered solution. Therefore, after being filtered, each sample was centrifuged at 13000 rpm speed for 10 minutes before measuring the absorbance.

3.1 Materials

3.1.1 UO_2 Powder

Hyper stoichiometric $\text{UO}_{2.3}$ powder [45] was procured by Westinghouse Electric Sweden AB. The specific surface area of the powder was determined as $5.4 \pm 0.2 \text{ m}^2 \cdot \text{g}^{-1}$ in a previous study [45].

3.1.2 Instrumentation and Software

The ultrapure water (resistivity of 18.2 $\text{M}\Omega \cdot \text{cm}$) was obtained from the Merck Millipore (Milli-Q, Type 1) to be used during experiments. Before absorbance measurements, the Thermo Scientific (Megafuge 16) centrifuge was used to aggregate particles with sizes smaller than 0.22 μm . In order to measure H_2O_2 and UO_2^{2+} absorbance values, the Thermo Scientific (the model of Genesys 20) spectrophotometer was used. The measurements were conducted at 360 nm to determine the I_3^- concentration as an indicator for H_2O_2 , while the wavelength was set to 653 nm for the determination of UO_2^{2+} concentration. Thermo Scientific (Orion Star A211) was used to measure the pH.

The Spana program [7, 53] was used to examine the H_2O_2 species formed in the systems having H_2O_2 , UO_2^{2+} and HCO_3^- .

3.2 Methodology

3.2.1 Ghormley Triiodide Method

H_2O_2 concentration was determined indirectly from the Ghormley Triiodide Method. This method was modified by Frew et al. (1983) [54] from the studies conducted by Allen et al. (1952) [55]. The primary purpose of the method is to determine the peroxide concentration in the aqueous systems by oxidation of potassium iodide (KI) by H_2O_2 in the presence of the ammonium molybdate ($(\text{NH}_4)_2\text{MoO}_4$) catalyst.

In this study, the peroxide concentration was calculated indirectly from the triiodide absorbance from Reaction 3.1 and Reaction 3.2 [7];



According to Reactions 3.1 and 3.2, the consumption of 1 mol of H_2O_2 (not only free H_2O_2 , but also peroxide complexes) corresponds to the production of 1 mol of I_3^- .

In this study, 360 nm was set in order not to overlap with the absorbance of UO_2^{2+} different than the experiments conducted at 352 nm by Frew et al. (1983) [54].

3.2.2 Arsenazo III Method

The Arsenazo III reagent (1,8-dihydroxynaphthalene-3,6-disulphonic acid-2,7-bis[azo-2]-phenylarsonic acid) is used for photometric detection of uranium (U), including some other elements such as thorium (Th), zirconium (Zr), hafnium (Hf) [56].

The region of optimum pH values for the interaction of Arsenazo III reagent with elements is known to vary. For the determination of Arsenazo III reagent ions, a significant degree of selectivity is achieved in a strongly acidic environment [56]. Therefore, the analysis were conducted in an acidic medium (in hydrochloric acid (HCl)) to eliminate the need to adjust pH with a buffer solution.

Although it is known that oxidizing and reducing agents attack the Arsenazo III reagent [56], Arsenazo III was used in this experiment with the presence of H_2O_2 which is oxidizing agents.

In this study, the wavelength was set at 653 nm in the spectrophotometer for UO_2^{2+} determination.

Chapter 4

Experimental Procedure

Experiments were performed to observe the oxidative dissolution of UO_2 in HCO_3^- solution in the presence of H_2O_2 . All experiments were conducted at room temperature with 50 mg $\text{UO}_{2.3}$ powder in 30 mL total solution volume (constant surface area to volume ratio).

The data for the systems with 10 mM HCO_3^- and 0.2 mM H_2O_2 were taken from a study by Olsson et al. (2022) [7].

4.1 Washing of powder

The washing step was done to remove the pre-oxidized UO_2 powder surface. Approximately 50 mg UO_2 powder was added into a 30 mL, 10 mM NaHCO_3 solution. The mixture was stirred with a magnetic stirrer under 1400 rpm for 15 s and waited 20 min for sedimentation. This step was repeated 3 times with a fresh HCO_3^- solution under N_2 purging. The mixture was stored in a glove box overnight with a sealed lid.

The next day, the washing step was repeated until UO_2^{2+} was no longer detectable (detection limit is $< 1 \mu\text{M}$).

4.2 Preparation of stock solutions and reagents

5 mL, 0.1 M H_2O_2 stock solution was prepared. The concentration of the H_2O_2 stock solution was measured 3 times before each experiment, and it was diluted to 0.2 mM to use in the experiments. Similarly, 5 mL, 0.1 M UO_2^{2+} solution was prepared from $\text{UO}_2(\text{NO}_3)_2 \times 6\text{H}_2\text{O}$ powder. Before each experiment, the solution was diluted to 0.3 mM. Finally, 1 L, 10 mM HCO_3^- solution was prepared from NaHCO_3 powder to be diluted to the desired concentrations (1 mM, 2 mM, 5 mM, and 10 mM) for each experiment.

In order to measure H_2O_2 concentration, 5 mL, 1 M KI solution was prepared. Apart from that, 50 mL, 2 M sodium acetate ($\text{C}_2\text{H}_3\text{NaO}_2$) and 50 mL, 2 M acetic acid (CH_3COOH) solutions were prepared, and mixed together. 50 drops of $(\text{NH}_4)_2\text{Mo}_2\text{O}_7$ catalyst were added to the mixture of $\text{C}_2\text{H}_3\text{NaO}_2$ and CH_3COOH so that the total volume was 100 mL [7].

On the other hand, 50 mL, 16 wt% Arsenazo III reagent solution, and 1 M HCl solution were prepared for the measurement of UO_2^{2+} concentration.

The sodium acetate/acetic acid/catalyst solution, the HCl solution, and an Arsenazo III were used throughout the experiments, while a fresh KI solution was prepared prior to each experiment and was not used for more than 7 hours. The solutions were stored in the dark storage as sealed when not in use.

4.3 UO_2 powder exposure

All experiments were conducted in the 50 mL cylindrical glass vessel sealed with a plastic septum under N_2 purging. The reason of N_2 purging is to prevent oxidation of UO_2 by air. In order to balance the inside and the outside pressure of the vessel, syringe needles were used. The reason for using syringe needles is to minimize the inclusion of air by using a smaller openings.

After removing the washing solution at the end of the washing steps described in Section 4.1, washed UO_2 powder was added into the 50 mL glass vessel together with the different concentrations of the HCO_3^- solution (1 mM, 2 mM, 5 mM, and 10 mM), separately. For each HCO_3^- concentration, experiments were conducted with and without initially added 0.3 mM UO_2^{2+} solution to vary the H_2O_2 species. The exposure started with the timer when 0.2 mM H_2O_2 was added to the glass vessel. The experiment parameters are presented in Table 4.1.

In order to determine the concentrations of H_2O_2 and UO_2^{2+} , approximately 1 mL of sample was taken with a syringe at regular intervals and filtered.

Table 4.1: Experimental conditions.

Sample	[HCO ₃ ⁻]/ mM	[H ₂ O ₂] [*] / mM		[UO ₂ ²⁺]/ mM	
		Targeted	Measured ^{**}	Targeted	Measured ^{**}
Sample 1	10	0.2	0.15	0	-
Sample 2	10	0.2	0.19	0.3	0.3
Repetition 2	10	0.2	0.13	0.3	0.25
Sample 3	5	0.2	0.16	0	-
Repetition 3	5	0.2	0.16	0	-
Sample 4	5	0.2	0.16	0.3	0.26
Repetition 4	5	0.2	0.19	0.3	0.27
Sample 5	2	0.2	0.14	0	-
Repetition 5	2	0.2	0.13	0	-
Sample 6	2	0.2	0.17	0.3	0.27
Repetition 6	2	0.2	0.16	0.3	0.27
Sample 7	1	0.2	0.14	0	-
Repetition 7	1	0.2	0.14	0	-
Sample 8	1	0.2	0.18	0.3	0.27

^{*}The H₂O₂ includes not only free H₂O₂ but also peroxide complexes.

^{**}The data measured after 0.5 min of exposure was indicated as "measured".

In the systems with 1 mM HCO₃⁻ and 2 mM HCO₃⁻, approximately 0.1 M sodium perchlorate (NaClO₄) was added into the samples after filtering, and samples were centrifuged before measuring the absorbance of the samples. The reason for adding ClO₄⁻ is to reduce the repulsion between equally charged surfaces so that particles are separated from the solution by precipitation. ClO₄⁻ was not added into the system with 5 mM HCO₃⁻ and 10 mM HCO₃⁻ since it was reported the complexation is a major effect rather than ionic strength in 10 mM HCO₃⁻ [26, 27].

100 μ L of KI solution, 100 μ L of sodium acetate/acetic acid/catalyst mixture, and 100 μ L (or sometimes 200 μ L, depending on the concentration) of the filtered sample were mixed and diluted to 2 mL of total cuvette volume. The H₂O₂ concentration was calculated using a calibration curve determined in a previous work [7].

On the other hand, 40 μ L of Arsenazo III reagent solution, 60 μ L of 1 M HCl solution, and 100 μ L (or sometimes 200 μ L, depending on the concentration) of the filtered sample were mixed and diluted to the total cuvette volume of 1.6 mL to measure the UO₂²⁺ concentration. UO₂²⁺ concentration was calculated using a calibration curve determined in a previous work [7].

Chapter 5

Results and Discussion

5.1 Oxidative Dissolution of UO_2

In order to investigate the effect of HCO_3^- concentration on the oxidative dissolution of UO_2 , the experiments were conducted by varying HCO_3^- concentration to 10 mM, 5 mM, 2 mM, and 1 mM in the presence of 0.2 mM H_2O_2 . The impact of H_2O_2 speciation on the dissolution kinetics was also analyzed by initially adding 0.3 mM UO_2^{2+} into the solutions. The experimental conditions are presented in Table 4.1.

Various H_2O_2 complexes were formed in the uranyl-peroxide-carbonate system, which will be discussed in Section 5.4. Therefore, the concentration of H_2O_2 mentioned includes not only free H_2O_2 but also peroxide complexes as a form of $(\text{UO}_2)_x(\text{O}_2)_y(\text{CO}_3)_z^{-a}$ and peroxide containing complexes as a form of $\text{UO}_2(\text{O}_2) \cdot 4\text{H}_2\text{O}$. Thus, the free H_2O_2 and peroxide complexes will be mentioned as H_2O_2 , and the total concentration of H_2O_2 will be illustrated as [peroxide] in this study.

The changes in the UO_2^{2+} concentration as a function of time for the systems with different HCO_3^- concentrations (10 mM, 5 mM, 2 mM, and 1 mM), 0.2 mM H_2O_2 without initially added UO_2^{2+} are presented in Figure 5.1 (a) and with initially added 0.3 mM UO_2^{2+} is presented in Figure 5.1 (b).

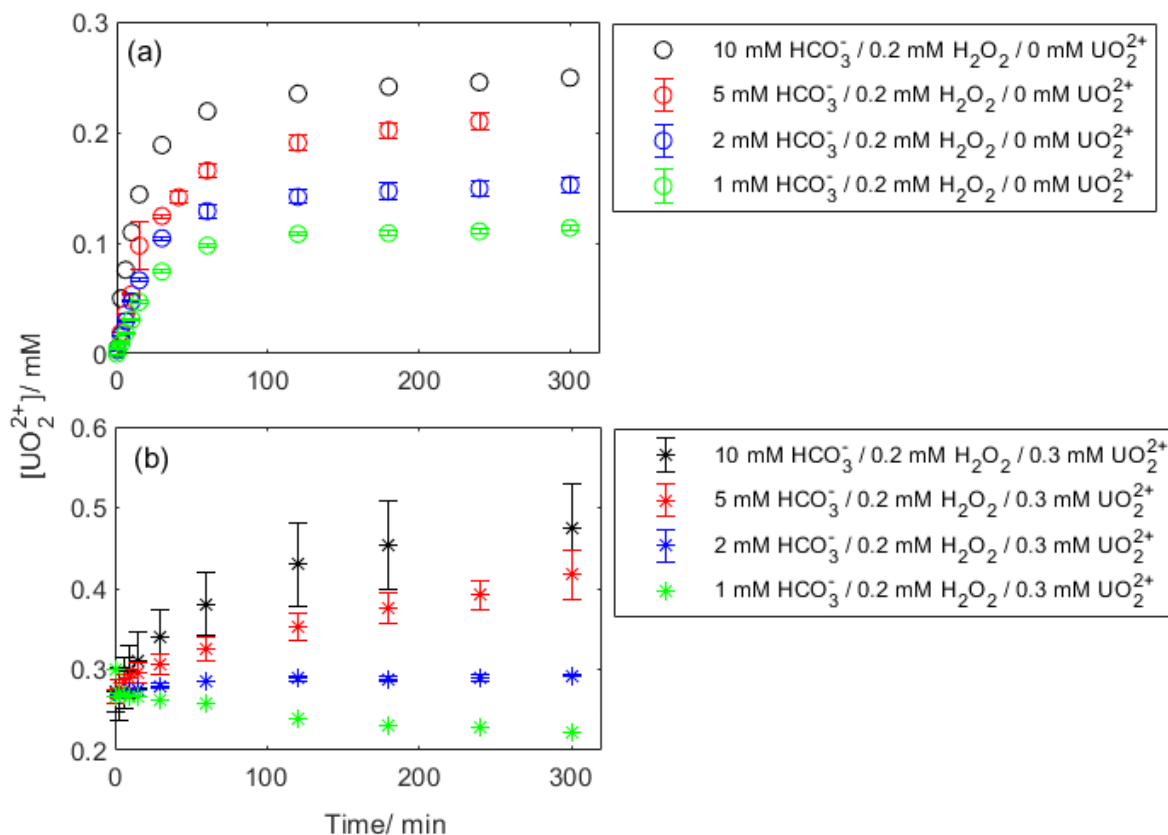


Figure 5.1: UO_2^{2+} concentration as a function of time in the systems that have 0.2 mM H_2O_2 , and 10 mM, 5 mM, 2 mM, and 1 mM HCO_3^- (a) without initially added UO_2^{2+} (b) with initially added 0.3 mM UO_2^{2+}

It can be seen in Figure 5.1 that there is an increasing trend in UO_2^{2+} concentration with time in the systems with different HCO_3^- concentrations except for the systems with 1 mM and 2 mM HCO_3^- with initially added 0.3 mM UO_2^{2+} . There is almost no UO_2^{2+} dissolution in the system having 2 mM HCO_3^- with initially added 0.3 mM UO_2^{2+} , while the UO_2^{2+} concentration decreases with time in the system having 1 mM HCO_3^- with initially added 0.3 mM UO_2^{2+} .

Figure 5.1 (a) shows that the UO_2^{2+} concentration stabilizes approximately 150 min after starting the exposure in the systems with different HCO_3^- concentrations without initially added UO_2^{2+} . The UO_2^{2+} concentrations are 0.25 mM, 0.21 mM, 0.15 mM, 0.11 mM for the systems with 10 mM HCO_3^- , 5 mM HCO_3^- , 2 mM HCO_3^- , and 1 mM HCO_3^- , respectively.

On the other hand, the UO_2^{2+} concentrations continue to increase in the systems with 10 mM HCO_3^- and 5 mM HCO_3^- with initially added UO_2^{2+} even after 300 min of exposure. The UO_2^{2+} concentration reaches 0.47 mM, 0.42 mM, 0.29 mM, 0.21 mM at 300 min of exposure for the systems with 10 mM HCO_3^- , 5 mM HCO_3^- , 2 mM HCO_3^- , and 1 mM HCO_3^- with initially added UO_2^{2+} , respectively.

In Figure 5.1 (b), the error percentage is high in the system having 10 mM HCO_3^- , 0.2 mM H_2O_2 and 0.3 mM UO_2^{2+} since the initial conditions of the two experiments being compared were different as presented in Table 4.1.

Both graphs in Figure 5.1 illustrate that increase in the UO_2^{2+} concentration is higher in higher HCO_3^- concentration as expected because HCO_3^- minimizes the risk for accumulation of dissolution products on the UO_2 surface, allowing UO_2^{2+} to be dissolved according to Reaction 2.3.

The dissolution of UO_2^{2+} is faster for the system without initially added UO_2^{2+} in Figure 5.1 (a) than the system with initially added UO_2^{2+} in Figure 5.1 (b) throughout the exposure. This is because the free H_2O_2 concentration is higher in the system without initially added UO_2^{2+} , and there are mostly H_2O_2 complexes in the system with initially added UO_2^{2+} . H_2O_2 speciation will be discussed in Section 5.4.

Figure 5.2 illustrates the change in the UO_2^{2+} and peroxide concentrations as a function of time in the systems with 10 mM HCO_3^- (a), 5 mM HCO_3^- (b), 2 mM HCO_3^- (c), 1 mM HCO_3^- (d) without initially added UO_2^{2+} . The H_2O_2 concentration in the graphs includes not only free H_2O_2 but also the H_2O_2 complexes.

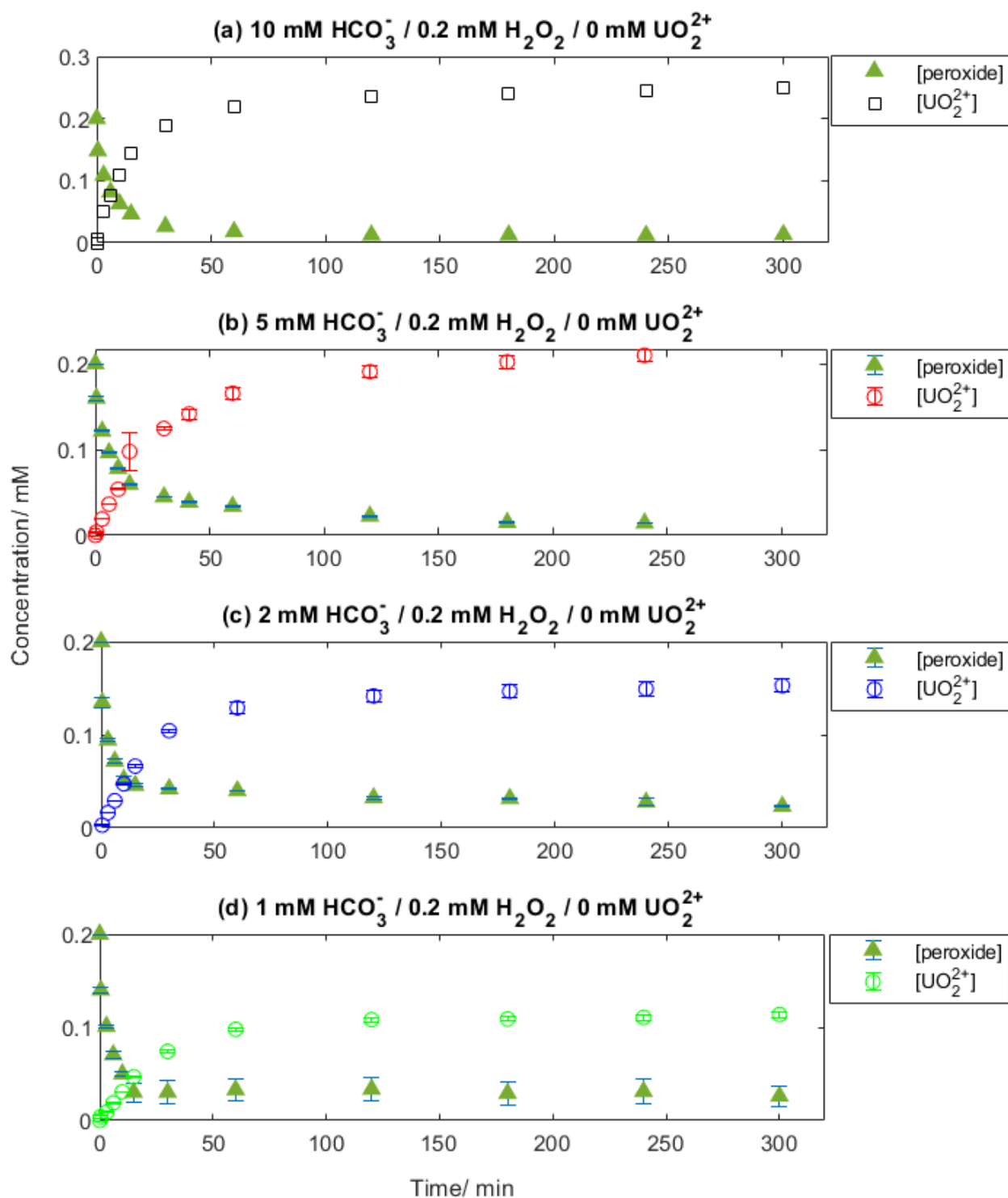


Figure 5.2: UO_2^{2+} and the peroxide concentrations as a function of time in the systems; (a) 10 mM HCO_3^- , (b) 5 mM HCO_3^- , (c) 2 mM HCO_3^- , (d) 1 mM HCO_3^- with 0.2 mM H_2O_2 and without initially added UO_2^{2+}

The maximum UO_2^{2+} concentration in the system with 10 mM HCO_3^- (0.25 mM) and 5 mM HCO_3^- (0.21 mM) is higher than the initial H_2O_2 concentrations. These indicate that there was pre-oxidized surface before starting the exposures.

The peroxide concentrations are 0.01 mM, 0.01 mM, 0.02 mM and 0.03 mM at 300 min of exposure for the systems with 10 mM HCO_3^- , 5 mM HCO_3^- , 2 mM HCO_3^- , and 1 mM HCO_3^- without initially added 0.3 mM UO_2^{2+} , respectively. Even though the amount of H_2O_2 consumed is similar for the systems with different HCO_3^- concentrations, less UO_2^{2+} dissolves in the system with lower HCO_3^- concentration. This may be attributed to the deficiency in HCO_3^- causes the accumulation of complexes and ions on the UO_2 surface, which blocks the dissolution of UO_2^{2+} from the UO_2 surface. There are no observable limitations for H_2O_2 consumption.

The UO_2^{2+} concentration was calculated by subtracting the initially added UO_2^{2+} concentration from the concentration measured at a particular time in the system with initially added UO_2^{2+} to compare the results with Figure 5.2. The results are illustrated in Figure 5.3 with the change in the peroxide concentration as a function of time in the systems with 10 mM HCO_3^- (a), 5 mM HCO_3^- (b), 2 mM HCO_3^- (c), 1 mM HCO_3^- (d).

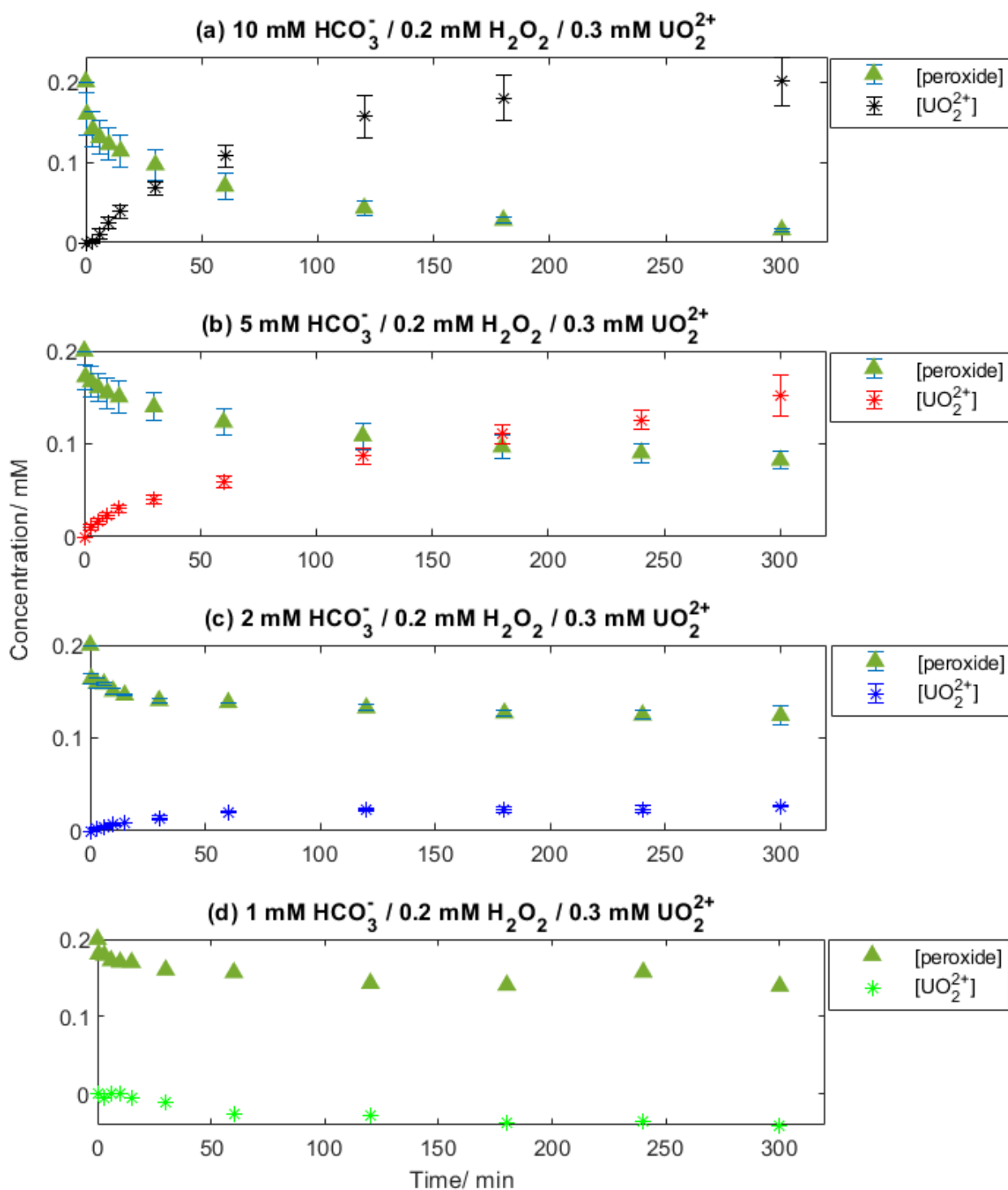


Figure 5.3: The UO_2^{2+} concentration (the concentration at time t subtracted from the initial concentration) and the peroxide concentration as a function of time in the systems with initially added UO_2^{2+} , 0.2 mM H_2O_2 ; (a) 10 mM HCO_3^- , (b) 5 mM HCO_3^- , (c) 2 mM HCO_3^- , (d) 1 mM HCO_3^-

It can be seen that the UO_2^{2+} concentration increases with decreasing peroxide concentration in the systems with 10 mM and 5 mM HCO_3^- with initially added 0.3 mM UO_2^{2+} in Figure 5.3 (a, b). Additionally, the reaction continues even after 300 min of exposure in these systems. On the other hand, the UO_2^{2+} concentration decreases in Figure 5.3 (d). This can be attributed to the studtite formation in the system with 1 mM HCO_3^- .

It can be seen from Figure 5.3 that the amount of peroxide consumed and UO_2^{2+} dissolved are less in the systems with initially added UO_2^{2+} than without initially added UO_2^{2+} (Figure 5.2).

The rate of peroxide consumption and UO_2^{2+} dissolution is less in the system with initially added UO_2^{2+} (Figure 5.3) than without initially added UO_2^{2+} (Figure 5.2). Therefore, it can be concluded that the presence of H_2O_2 complexes decelerates the H_2O_2 consumption and UO_2^{2+} dissolution in the system with initially added UO_2^{2+} . Olsson et al. (2022) reported similar results in their study by varying the UO_2^{2+} concentrations as 0 mM, 0.3 mM and 0.58 mM [7].

In all the graphs in Figure 5.3, a delay can be seen in the UO_2^{2+} dissolution compared with H_2O_2 consumption. This delay is because the H_2O_2 must first oxidize the UO_2 surface, and then the UO_2^{2+} formed with oxidation must be dissolved from the surface.

de Pablo et al. (2000) [57] conducted an experiment with different H_2O_2 concentrations (from 10^{-5} M to 10^{-3} M) and reported that H_2O_2 consumption was faster than UO_2^{2+} dissolution. They have interpreted that the dissolution of UO_2^{2+} is the rate limiting factor for oxidative dissolution of UO_2 under their experimental conditions.

On the other hand, the lower HCO_3^- concentration can also delay or even stop the dissolution of the UO_2^{2+} . HCO_3^- accelerates the UO_2^{2+} dissolution from the surface since HCO_3^- mitigates the accumulation of complexes on the solid surface. Therefore, Reaction 2.3 becomes the rate limiting step instead of Reaction 2.1 in the deficiency of HCO_3^- [2, 26]. It can be seen from Figure 5.2 and Figure 5.3 that less UO_2^{2+} is dissolved in the system with lower HCO_3^- concentration.

The concentration of UO_2^{2+} as a function of time for the systems having different HCO_3^- concentrations, 0.2 mM H_2O_2 with and without initially added 0.3 mM UO_2^{2+} is presented in Figure 5.4. The initially added UO_2^{2+} was subtracted from the concentration measured at a particular time.

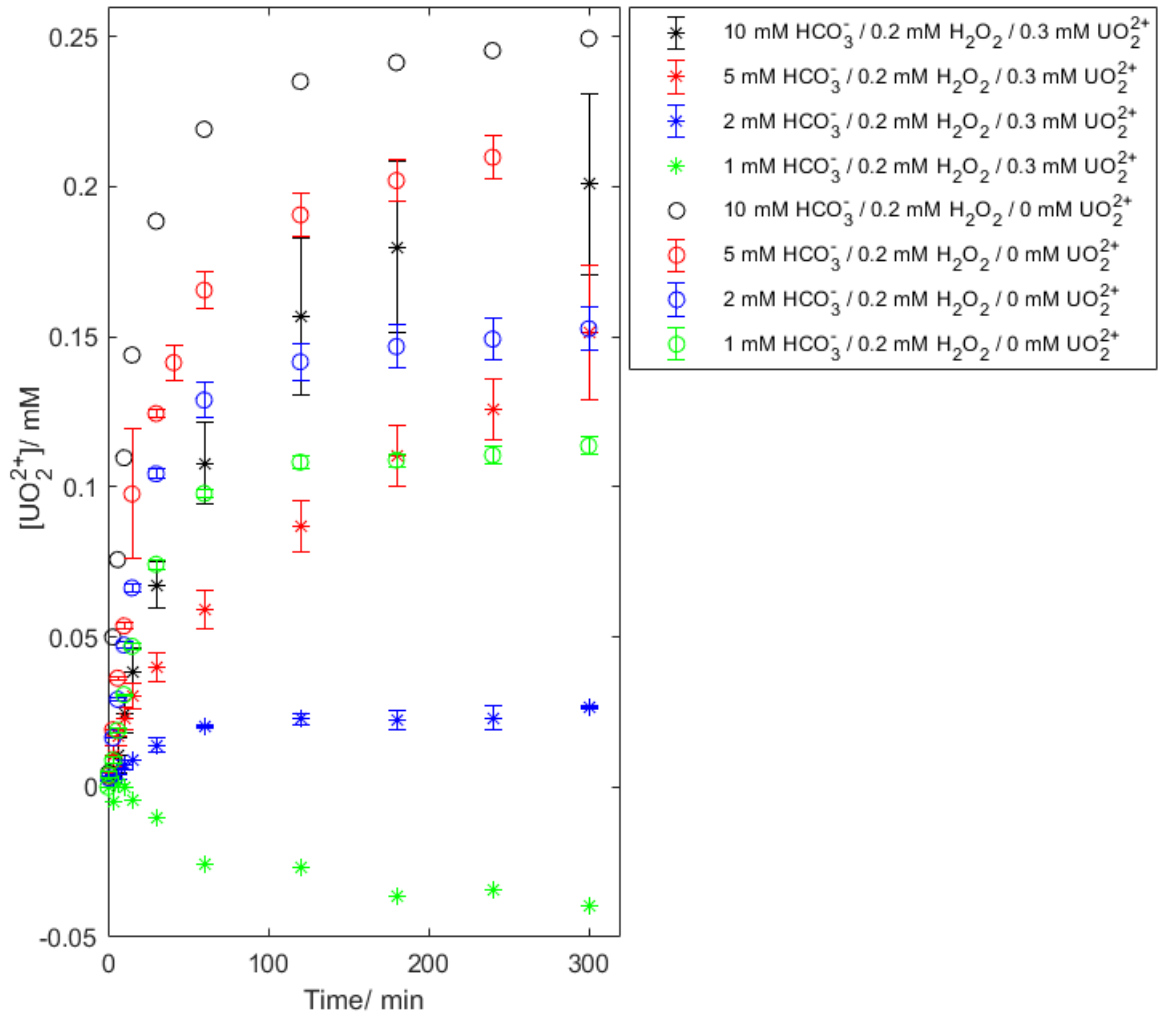


Figure 5.4: UO_2^{2+} concentration as a function of time in the systems that have 0.2 mM H_2O_2 , and 10 mM, 5 mM, 2 mM and 1 mM HCO_3^- with and without initially added 0.3 mM UO_2^{2+}

If the systems with and without initially added UO_2^{2+} are compared separately, it can be seen that the UO_2^{2+} dissolution is high in high HCO_3^- concentration. On the other hand, when the systems that have the same HCO_3^- concentration are analyzed together, it is clear that the dissolution of UO_2^{2+} in the system without initially added UO_2^{2+} is higher than that of the system with initially added UO_2^{2+} .

5.2 Long-Term Oxidative Dissolution of UO_2

Since there was still H_2O_2 in the systems with different HCO_3^- concentrations with initially added UO_2^{2+} , and 1 mM and 2 mM HCO_3^- without initially added UO_2^{2+} , the exposures were run for longer time. In order to understand the long-term trend of oxidative dissolution of UO_2 , the change in the H_2O_2 and UO_2^{2+} concentration as a function of time are illustrated in Figure 5.5 (a) and (b), respectively.

In the experiments that were conducted for a prolonged period, solid particles were observed in the sample after filtering. This may be because the solid breaks down mechanically as it mixes in the stirrer. Therefore, it should be considered that the surface area of the solid may increase over time.

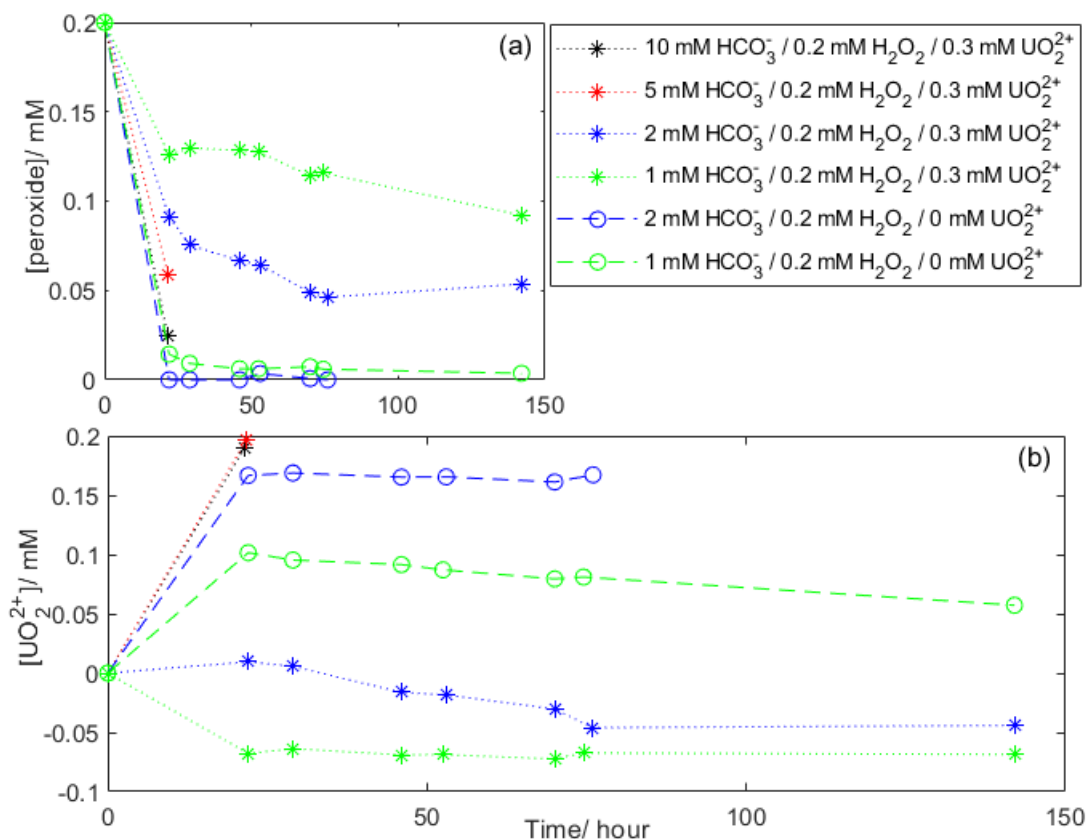


Figure 5.5: Concentrations of (a) H_2O_2 , (b) UO_2^{2+} as a function of time for the systems have 0.2 mM H_2O_2 , and 10 mM, 5 mM, 2 mM, and 1 mM HCO_3^- , with initially added 0.3 mM UO_2^{2+} ; and 2 mM and 1 mM HCO_3^- , 0.2 mM H_2O_2 without initially added UO_2^{2+}

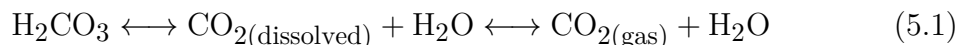
The experiments that have 10 mM HCO_3^- and 5 mM HCO_3^- , 0.2 mM H_2O_2 with initially added UO_2^{2+} were stopped after around 22 hours of exposure. Since there is still H_2O_2 (Figure 5.5 (a)), the experiments could have been continued for an extended period.

Figure 5.5 (a) illustrates that in the systems having 1 mM and 2 mM HCO_3^- , 0.2 mM H_2O_2 without initially added UO_2^{2+} , H_2O_2 is almost fully consumed at around 22 hours of exposure; therefore, there are no significant changes in UO_2^{2+} concentration for these systems as shown in Figure 5.5 (b).

On the other hand, H_2O_2 concentration decreases over time in the system with 2 mM HCO_3^- , 0.2 mM H_2O_2 and initially added 0.3 mM UO_2^{2+} as presented in Figure 5.5 (a). This may be due to studtite formation in this system after 22 hours of exposure.

Finally, in the system having 1 mM HCO_3^- with initially added 0.3 mM UO_2^{2+} , the H_2O_2 concentration decreases while there is no significant change in the UO_2^{2+} concentration. This may be because the HCO_3^- deficiency limits the dissolution capacity of the system. In other words, H_2O_2 continues to oxidize the UO_2 surface; however, there is no HCO_3^- in the system to clean the UO_2 surface from dissolution products for UO_2^{2+} dissolution. In order to analyze this system in more detail, HCO_3^- may be added, and whether there will be changes in the dissolution may be observed.

In long-term exposures, it should be considered that the CO_2 that is formed as in Reaction 5.1 is removed by N_2 purging. Therefore, the HCO_3^- concentration decreases further over time. In order to prevent this, the N_2 purging may be done through the HCO_3^- solution.



5.3 Oxidative Dissolution Effect on pH

The pH values for the systems with different HCO_3^- concentrations increase from roughly 6.5 to 10.5 throughout the exposures. The pH values measured for each system are presented in Table 1 - Table 8 in the Appendix. The pH values at a particular time necessary for the speciation calculation were determined from the polynomial function obtained from the fitted experimental data.

To emphasize the importance of the pH on the H_2O_2 speciation, Figure 5.6 is presented for the system with 5 mM HCO_3^- , 0.2 mM H_2O_2 with initially added 0.3 mM UO_2^{2+} . The figure was prepared in SPANA from the data (concentrations of H_2O_2 , UO_2^{2+} , and HCO_3^-) measured at 0.5 min, 60 min and 300 min of exposure, and the pH values. The yellow line represents the pH value obtained from the polynomial function fitting to experimental data, while the red line shows the pH obtained by averaging all pH values. The y-axis illustrates the fraction of H_2O_2 species as a fraction of the total H_2O_2 concentration in the system.

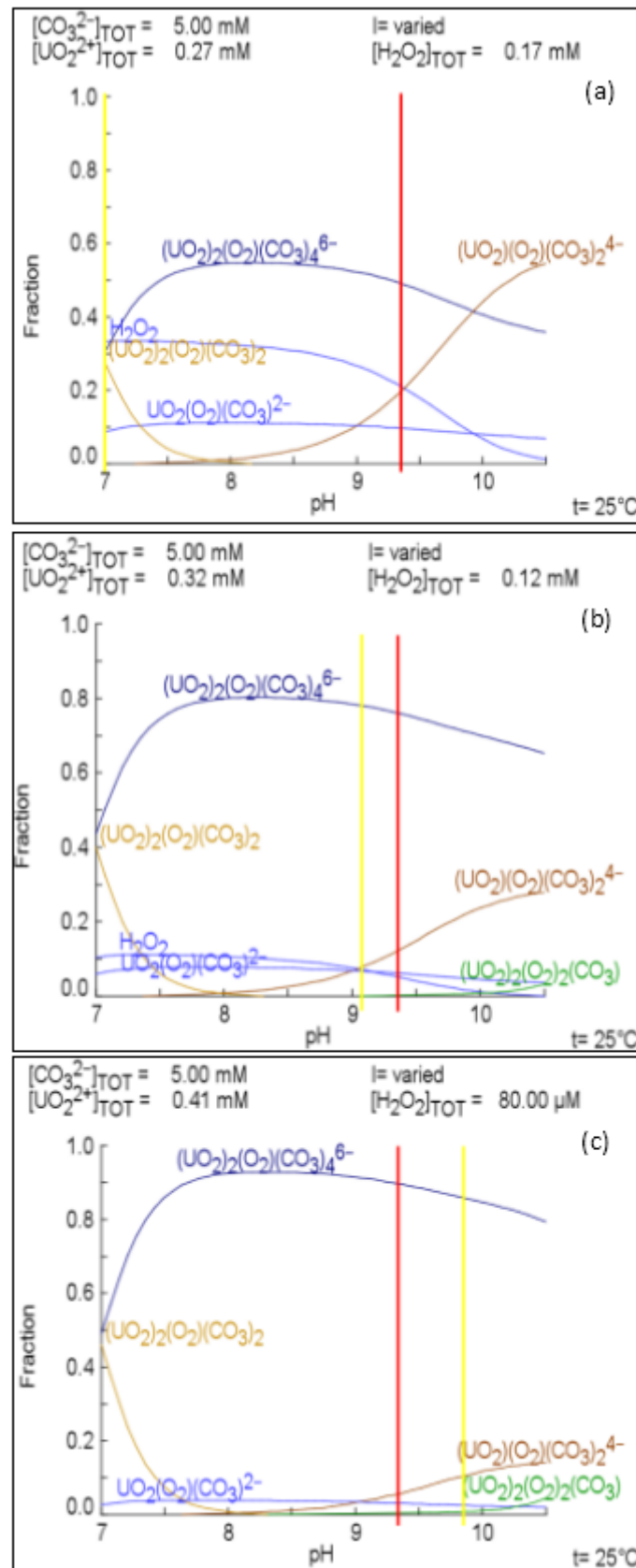


Figure 5.6: Speciation calculation prepared in SPANA with the data at (a) 0.5 min, (b) 60 min and (c) 300 min of exposure for the system with 5 mM HCO_3^- , 0.2 mM H_2O_2 with initially added 0.3 mM UO_2^{2+}

Since the pH mainly changes at the beginning of the exposure, the difference between the determined pH for a particular time ($\text{pH} \approx 7$) and the average pH ($\text{pH} \approx 9.4$) is higher at 0.5 min of exposure. Therefore, the fraction of the dominant complex changes significantly with pH at 0.5 min of exposure, as shown in Figure 5.6 (a). Since there is no significant change in the pH afterward, the fraction of dominant species is almost the same at both pH values.

As shown in Appendix, the pH values at the beginning of the exposure are lower than the rest of the exposure. The reason for the lower initial pH may be because of the addition of the H_2O_2 which is a weak acid [24]. The H_2O_2 concentration decreases with the dissolution of the UO_2 as illustrated in Figure 5.2 and Figure 5.3; therefore, the solutions became more alkali. There is no significant change in pH when H_2O_2 consumption reaches the maximum. Hou et al. (2022) reported the similar results [24].

Hou et al. (2022) [24] reported that the H^+ concentration increases with the complexation based on Reaction 2.6. This increase will lead to shift the reaction throughout the lower alkalinities. With the depletion of H_2O_2 , the production rate of H^+ slows down. In that case, the hydrolysis of CO_3^{2-} becomes more dominated, and H^+ production becomes slower according to Reaction 5.2 and Reaction 5.3. Therefore, the pH values in the systems increases.



5.4 Speciation Calculation

Speciation calculations were performed using the SPANA program [53] based on the concentrations of H_2O_2 , UO_2^{2+} , HCO_3^- , and pH values presented in the tables in Appendix. The program automatically corrected the ionic strength based on a simple Helgeson-Krikham-Flowers Model.

The average pH values were used for speciation calculation for the systems that have 10 mM HCO_3^- both with and without initially added UO_2^{2+} since there is no significant change in the fraction of H_2O_2 species with the pH range measured.

Extra pH values needed for speciation calculation were obtained from the polynomial function obtained from the fitted experimental data for the systems with 5 mM HCO_3^- , 2 mM HCO_3^- and 1 mM HCO_3^- . The detailed speciation calculation as a fraction of the total H_2O_2 concentration for the system with different HCO_3^- concentrations without initially added UO_2^{2+} is presented in Figure 5.7.

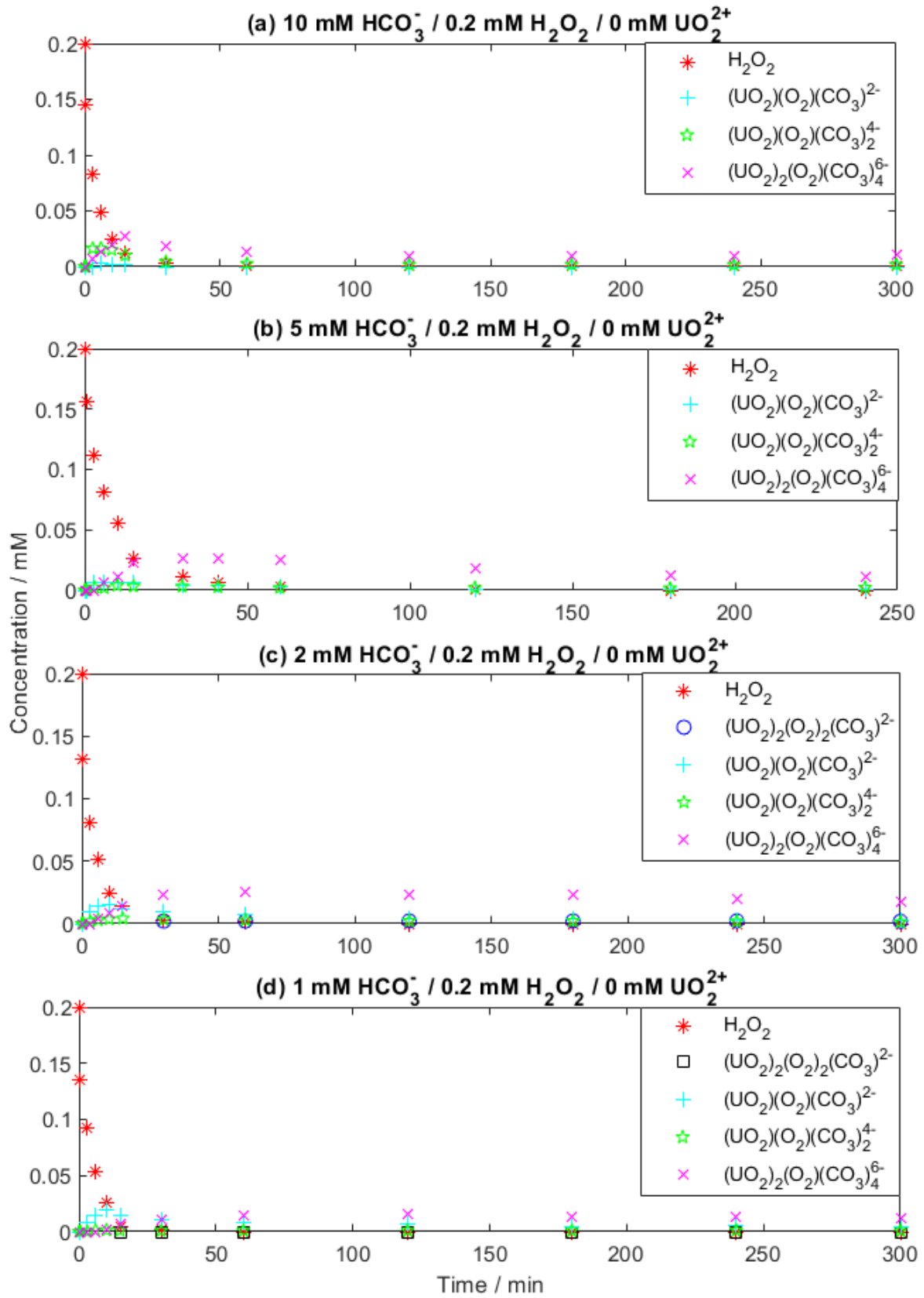


Figure 5.7: Concentration of the H_2O_2 species calculated from SPANA as a function of time for the systems that have 0.2 mM H_2O_2 , and (a) 10 mM HCO_3^- , (b) 5 mM HCO_3^- , (c) 2 mM HCO_3^- (d) 1 mM HCO_3^- without initially added UO_2^{2+}

The program incorrectly gave the charge of two complexes ($\text{UO}_2(\text{O}_2)_2(\text{CO}_3)$ and $\text{UO}_2(\text{O}_2)_2(\text{CO}_3)$) as 0 instead of -2. The charge of the complexes will be given as -2 in this study.

Figure 5.7 illustrates that there is mostly free H_2O_2 in the systems. The free H_2O_2 is almost fully consumed in 30 min of exposure in the systems with 10 mM (a), 2 mM (c), 1 mM HCO_3^- (d) without initially added UO_2^{2+} . On the other hand, there is still free H_2O_2 remained in the system with 5 mM HCO_3^- without initially added UO_2^{2+} at 60 min of exposure as shown in Figure 5.7 (b). The concentrations of the remained complexes change around 0.02 mM. Since most of the H_2O_2 is consumed at the beginning of the exposure, there is no significant change after consumption of free H_2O_2 . The results are similar with the peroxide consumption graphs in Figure 5.2.

The speciation calculation as a fraction of total H_2O_2 concentration for the system with different HCO_3^- concentrations with initially added 0.3 mM UO_2^{2+} is presented in Figure 5.8.

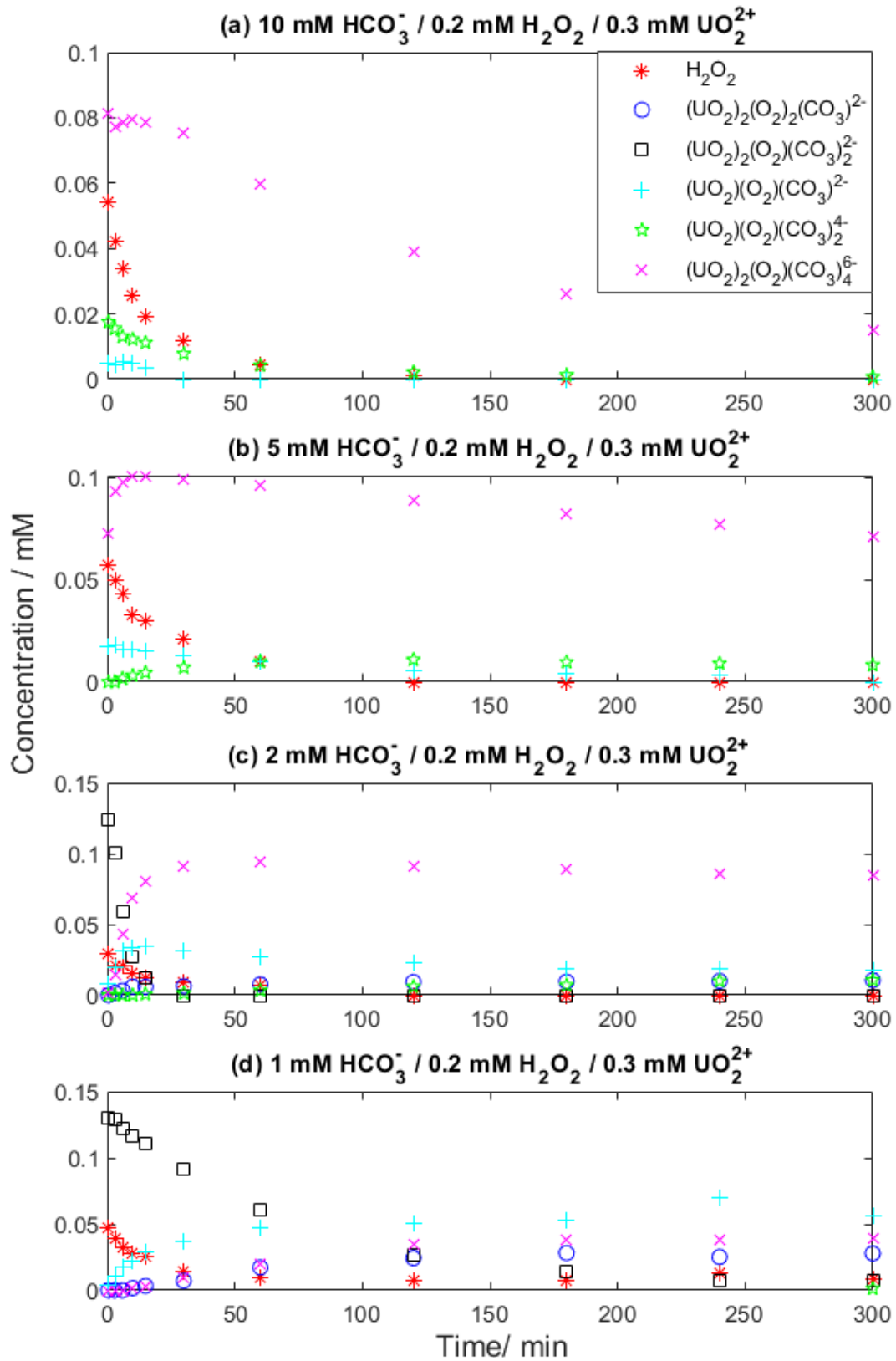


Figure 5.8: Concentration of the H_2O_2 species calculated from SPANA as a function of time for the systems that have 0.2 mM H_2O_2 , and (a) 10 mM HCO_3^- , (b) 5 mM HCO_3^- , (c) 2 mM HCO_3^- (d) 1 mM HCO_3^- with initially added 0.3 mM UO_2^{2+}

Speciation calculations enlighten that $(\text{UO}_2)_2(\text{O}_2)(\text{CO}_3)_4^{6-}$ is dominant H_2O_2 complex for the systems that have 10 mM, 5 mM and 2 mM HCO_3^- with initially added UO_2^{2+} as shown in Figure 5.8 (a-c).

El Jamal et al. (2021) [27] have reported that the reactivity of $(\text{UO}_2)_2(\text{O}_2)(\text{CO}_3)_4^{6-}$ is significantly lower than that of H_2O_2 towards UO_2 for the system with 10 mM HCO_3^- and 2 mM H_2O_2 .

In the system that has 1 mM HCO_3^- with initially added UO_2^{2+} , $(\text{UO}_2)_2(\text{O}_2)(\text{CO}_3)_2^{2-}$ is the dominant complex in the first 60 min as illustrated in Figure 5.8 (d). Meanwhile the second dominant species H_2O_2 resigns its predominance to $(\text{UO}_2)(\text{O}_2)(\text{CO}_3)^{2-}$, $(\text{UO}_2)_2(\text{O}_2)(\text{CO}_3)_4^{6-}$ and $(\text{UO}_2)_2(\text{O}_2)_2(\text{CO}_3)^{2-}$ after around 30 min of exposure.

It is clear that the speciation is more important for the system with initially added UO_2^{2+} (Figure 5.8) than without initially added UO_2^{2+} (Figure 5.7). Since the amount of free H_2O_2 remained in the system with initially added UO_2^{2+} is less than that of without initially added UO_2^{2+} , the amount of dissolved UO_2^{2+} is lower in the former, as discussed in Section 5.1.

Even though pH is important in speciation calculation, it is difficult to analyze which complex dominates the systems when pH is low or high in this study. The reason for this statement is that there is a rather significant change in pH only at the beginning of the experiments. Also, the pH range is similar for the systems with different HCO_3^- concentrations. The Pourbaix diagrams may be used to analyze the species formed at specific pH values.

As discussed in Section 2.3 and Section 5.2, the deficiency in HCO_3^- delays or even stops the UO_2^{2+} dissolution due to the accumulation of UO_2^{2+} ions or complexes on the UO_2 surface. Analyzing the HCO_3^- concentration during the experiments is difficult due to the possible different mechanisms that may intervene in the concentration changes, such as removing of CO_2 by N_2 purging as given in Reaction 5.1. However, assuming there is no intervening mechanism, the HCO_3^- concentrations at 300 min of exposure are calculated by SPANA using concentrations of H_2O_2 , UO_2^{2+} and HCO_3^- , and pH values. The results are given in Table 5.1 for different systems. As it can be seen that the $\text{HCO}_3^-/\text{CO}_3^{2-}$ is the majority among the other complexes.

Table 5.1: HCO_3^- speciation calculated from SPANA as a fraction of HCO_3^- for the systems that have 10 mM, 5 mM, 2 mM and 1 mM HCO_3^- , 0.2 mM H_2O_2 with and without initially added 0.3 mM UO_2^{2+} at 300 min of exposure.

System	$[\text{HCO}_3^-]/$ mM	$[\text{CO}_3^{2-}]/$ mM	$[\text{UO}_2(\text{CO}_3)_3^{4-}]/$ mM	$[\text{UO}_2(\text{O}_2)(\text{CO}_3)_4^{6-}]/$ mM
10 mM HCO_3^- , 0.3 mM UO_2^{2+}	7.4	1.3	1.3	
10 mM HCO_3^- , 0 mM UO_2^{2+}	6.5	2.8	0.7	
5 mM HCO_3^- , 0.3 mM UO_2^{2+}	1.95	1.95	0.85	0.25
5 mM HCO_3^- , 0 mM UO_2^{2+}	2.2	2.2	0.55	
2 mM HCO_3^- , 0.3 mM UO_2^{2+}	0.8	0.36	0.8	
2 mM HCO_3^- , 0 mM UO_2^{2+}	1.18	0.42	0.34	0.06
1 mM HCO_3^- , 0.3 mM UO_2^{2+}	0.4	0.02	0.52	
1 mM HCO_3^- , 0 mM UO_2^{2+}	0.59	0.15	0.19	0.05

*The main complexes formed are presented in the table. The complexes $(\text{UO}_2)_2(\text{O}_2)_2(\text{CO}_3)^{2-}$ and $\text{UO}_2(\text{CO}_3)_2^{2-}$ having relatively low concentrations in the systems are not presented in the table.

5.5 Kinetic Analysis

The H_2O_2 consumption and natural logarithm of H_2O_2 consumption in the first 15 min of exposure as a function of time for the systems with different HCO_3^- concentrations and without initially added UO_2^{2+} are shown in Figure 5.9 and Figure 5.10, respectively.

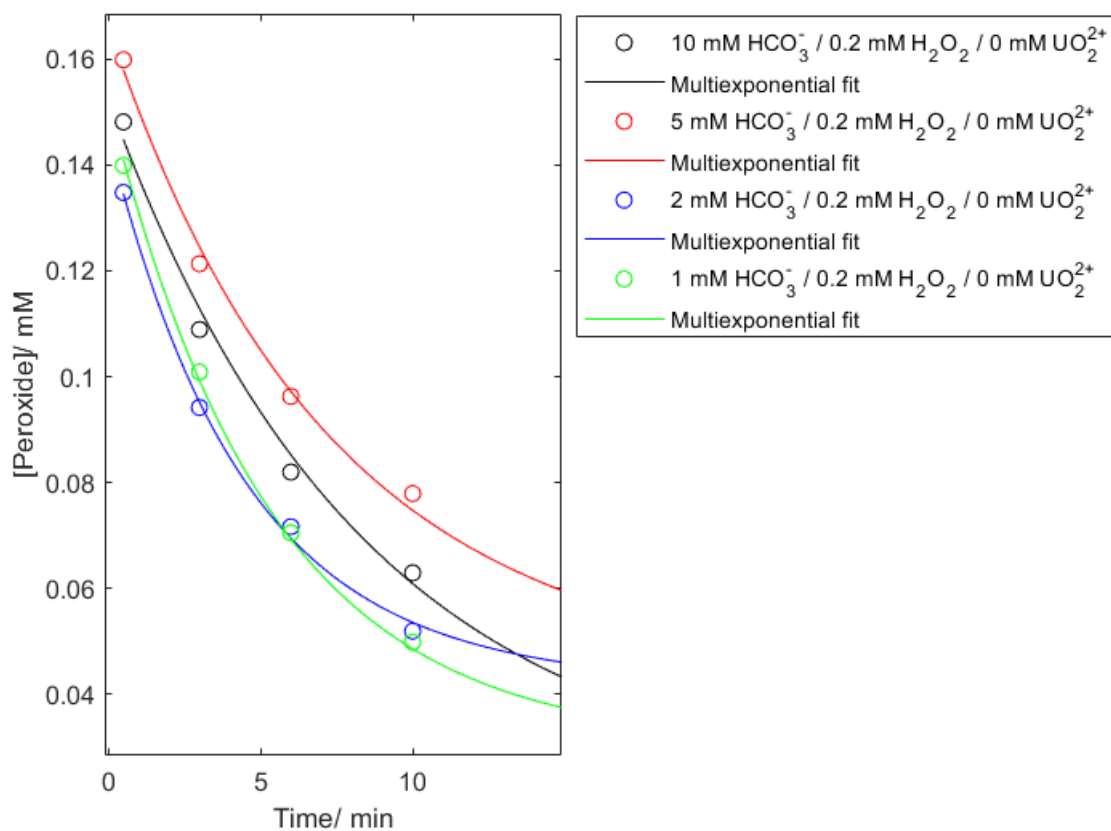


Figure 5.9: The H_2O_2 consumption in the first 15 min of exposure and its multi-exponential fit as a function of time for the systems with different HCO_3^- concentrations and without initially added UO_2^{2+}

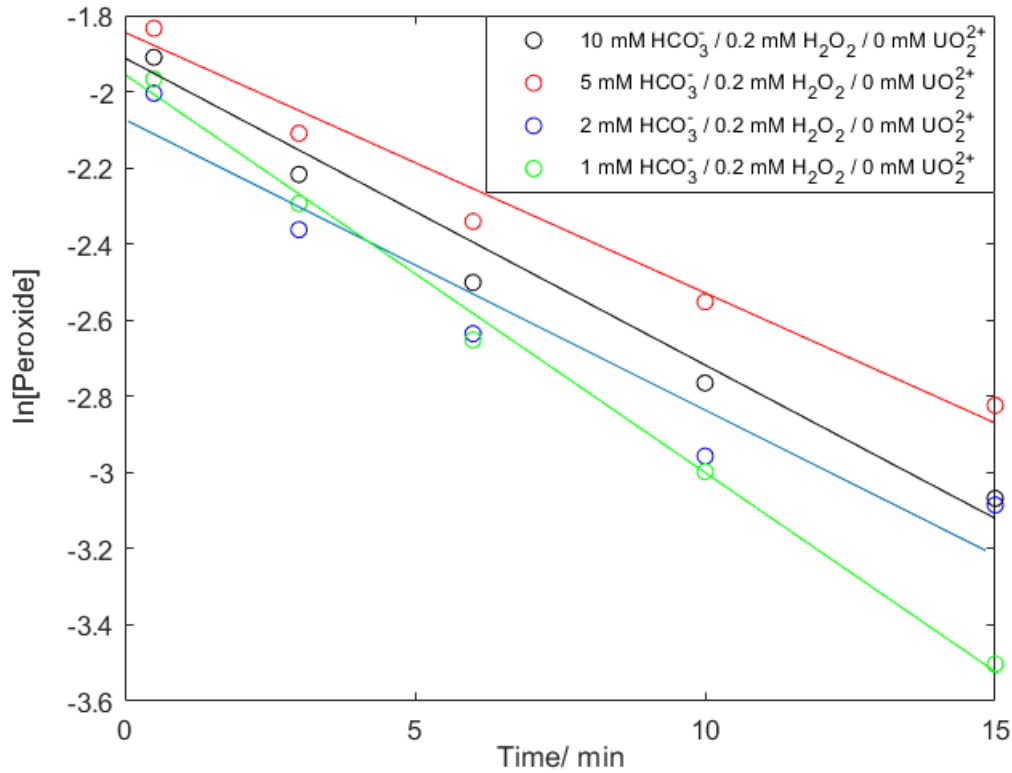


Figure 5.10: Natural logarithm of H_2O_2 consumption in the first 15 min of exposure as a function of time for the systems with different HCO_3^- concentrations and without initially added UO_2^{2+}

The H_2O_2 consumption rate was calculated from the minus derivative of free H_2O_2 concentration calculated from polynomial fitting at 0.5 min as given in Equation 5.4. The first-order rate constant was calculated from the slopes in Figure 5.10. Finally, the second-order rate constant was calculated from the normalization of first-order rate constant by surface area to volume ratio which is 9000 m^{-1} . The results are presented in Table 5.2.

$$\text{Rate} = -\frac{d[\text{H}_2\text{O}_{2,\text{free}}]}{dt} \quad (5.4)$$

Table 5.2: Free H_2O_2 concentration determined from SPANA for time = 0.5 min, the rate, the first-order and the second order rate constants for the systems with 0.2 mM H_2O_2 , different HCO_3^- concentrations without initially added UO_2^{2+} .

System	$[\text{H}_2\text{O}_{2,\text{free}}]/$ mM	Rate/ $\text{M}\cdot\text{s}^{-1}$	1 st order rate constant/ s^{-1}	2 nd order rate constant/ $\text{m}\cdot\text{s}^{-1}$
10 mM HCO_3^-	0.054	2.4×10^{-6}	0.0013	1.4×10^{-7}
5 mM HCO_3^-	0.057	2.1×10^{-6}	0.0011	1.2×10^{-7}
2 mM HCO_3^-	0.029	3.7×10^{-6}	0.0012	1.3×10^{-7}
1 mM HCO_3^-	0.047	3.0×10^{-6}	0.0017	1.9×10^{-7}

The H_2O_2 consumption rate and rate constants are similar for the systems with different HCO_3^- concentrations in Table 5.2. It can be seen that the H_2O_2 consumption kinetics is independent of HCO_3^- concentration for the system without initially added UO_2^{2+} .

More than 60% of the H_2O_2 is consumed in the first 15 min of exposure. From the discussion provided in Section 5.1, it was expected that the H_2O_2 consumption rate will increase with increasing HCO_3^- concentration since HCO_3^- removes the UO_2^{2+} ions and complexes from the UO_2 surface, which increases the dissolution of oxidized UO_2 . However, it can be seen in Figure 5.9 and Figure 5.10 that the H_2O_2 consumption rate is independent of HCO_3^- concentration. It can be explained by the surface area to H_2O_2 ratio. In this study, the surface area is a very large excess compared to H_2O_2 concentration. Therefore, the effect of HCO_3^- is less than the studies done with a high amount of H_2O_2 .

On the other hand, the H_2O_2 consumption in the first 15 min of exposure and its multi-exponential fit as a function of time for the systems with different HCO_3^- concentrations and with initially added 0.3 mM UO_2^{2+} are given in Figure 5.11.

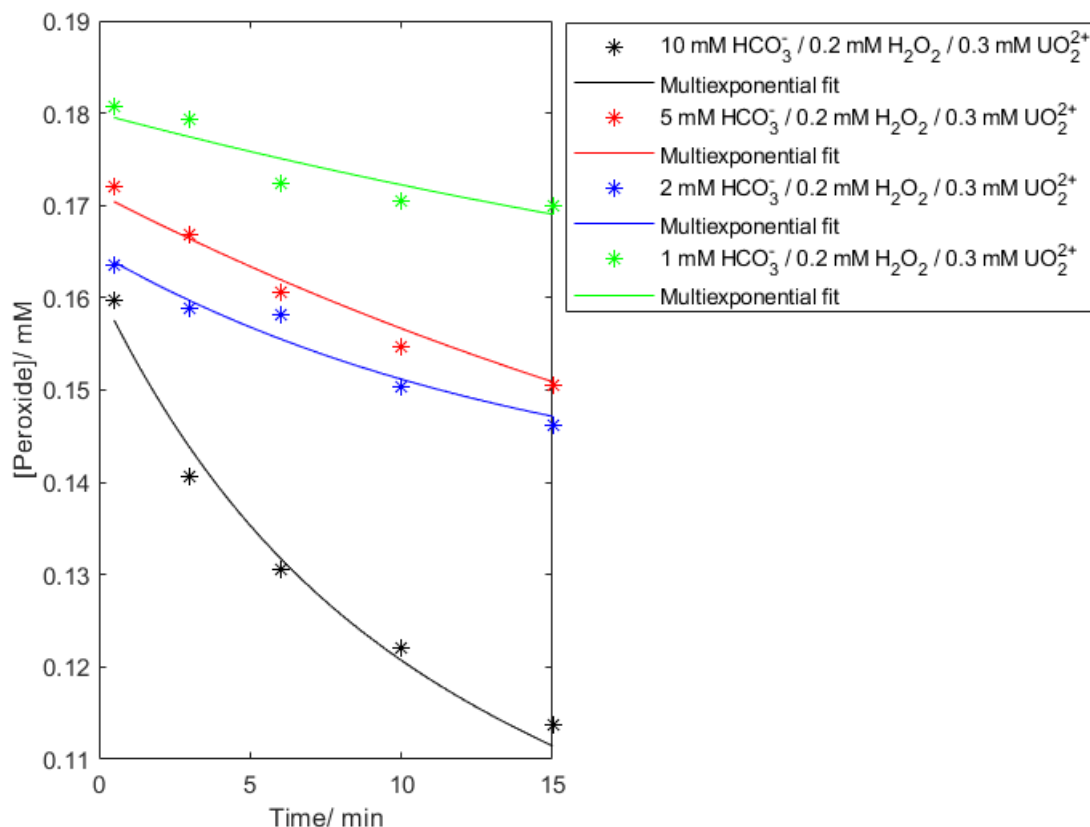


Figure 5.11: The H_2O_2 consumption in the first 15 min of exposure and its multiexponential fit as a function of time for the systems with different HCO_3^- concentrations and with initially added $0.3 \text{ mM } \text{UO}_2^{2+}$

Figure 5.11 illustrates that H_2O_2 consumption is slower for $1 \text{ mM } \text{HCO}_3^-$ followed by $5 \text{ mM } \text{HCO}_3^-$ and $2 \text{ mM } \text{HCO}_3^-$, and $10 \text{ mM } \text{HCO}_3^-$. It can be seen that there is no observable trend in H_2O_2 consumption rate with respect to HCO_3^- concentration. The deviation in the H_2O_2 consumption kinetics can be observed in $10 \text{ mM } \text{HCO}_3^-$. Therefore, it can be concluded that the H_2O_2 consumption kinetics is independent of HCO_3^- concentration in $5 \text{ mM } \text{HCO}_3^-$ and in lower HCO_3^- concentrations.

Hossain et al. (2006) [16] observed the H_2O_2 consumption kinetics in 18 mL suspension containing $50 \text{ mg } \text{UO}_2$ with $18 \text{ mM } \text{H}_2\text{O}_2$ and different HCO_3^- concentrations ($0\text{-}100 \text{ mM}$). It has been concluded that the H_2O_2 consumption increases with increasing HCO_3^- concentration. Also, the second-order rate constant has been reported as increasing with increasing HCO_3^- concentration of $0\text{-}1 \text{ mM}$, while as independent of HCO_3^- concentration in higher HCO_3^- concentrations. The reaction rate has been found as independent of dissolution of UO_2^{2+} .

UO_2^{2+} dissolution kinetics for the first 15 min of exposure for the systems with different HCO_3^- concentration without initially added UO_2^{2+} is given in Figure 5.12. The slopes of UO_2^{2+} dissolution curves are 0.57 , 0.28 , 0.23 , and 0.17 for the systems with 10 mM , 5 mM , 2 mM , and $1 \text{ mM } \text{HCO}_3^-$, respectively.

Considering experimental uncertainties, it can be concluded that the UO_2^{2+} dissolution rate is proportional to HCO_3^- concentration and follows first-order kinetics with respect to HCO_3^- concentration.

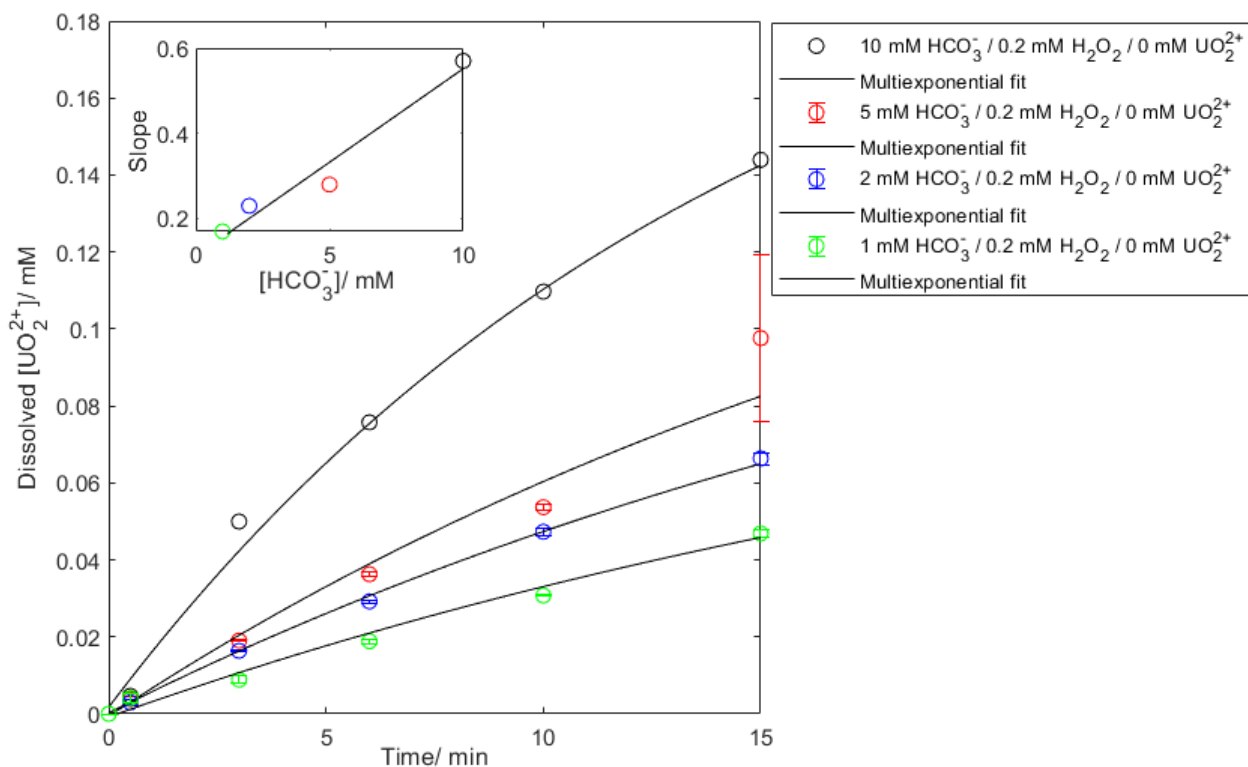


Figure 5.12: The UO_2^{2+} concentration in the first 15 min of exposure and its multiexponential fit as a function of time for the systems with different HCO_3^- concentrations and without initially added UO_2^{2+}

UO_2^{2+} dissolution kinetics for the first 15 min of exposure for the systems with different HCO_3^- concentration with initially added 0.3 mM UO_2^{2+} is given in Figure 5.13.

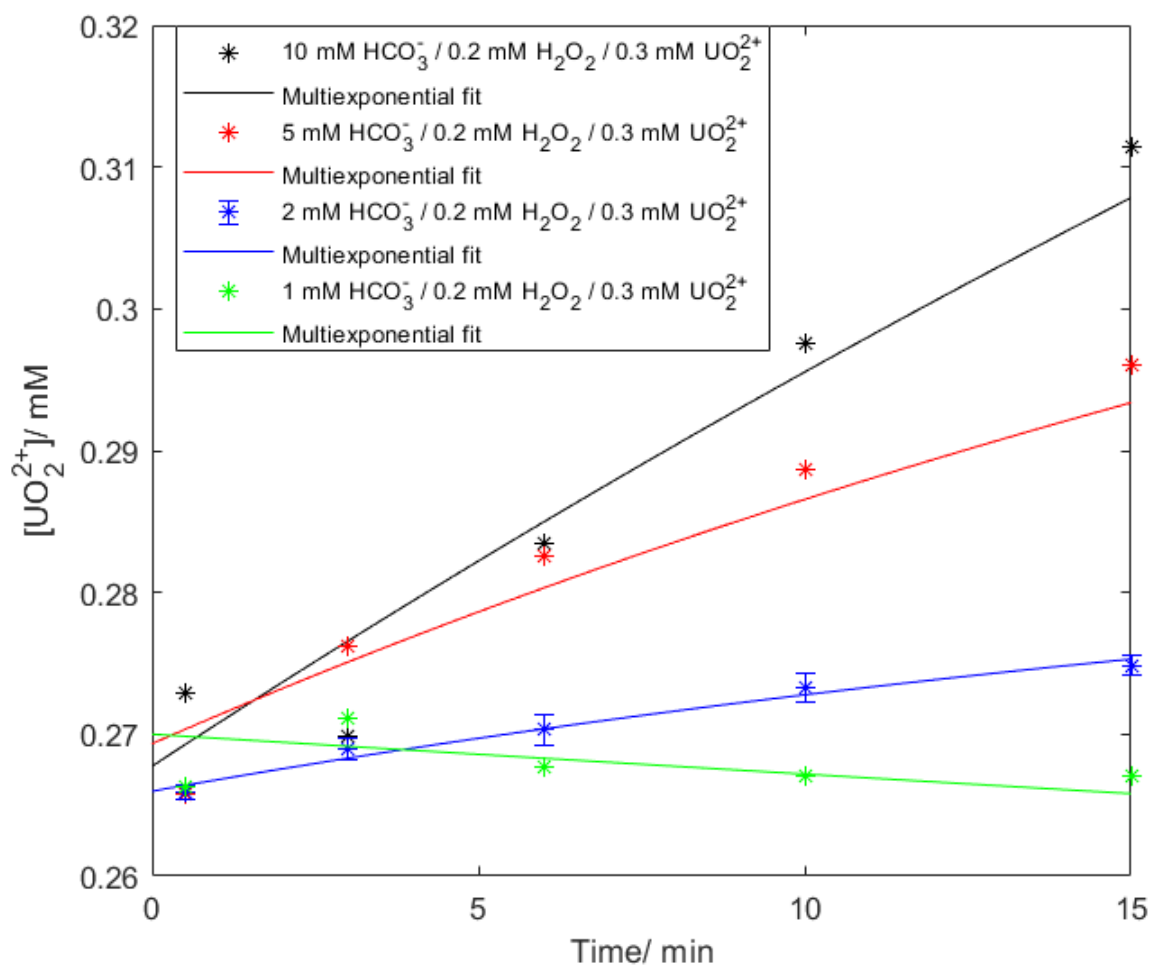


Figure 5.13: The UO_2^{2+} concentration in the first 15 min of exposure and its multiexponential fit as a function of time for the systems with different HCO_3^- concentrations and with initially added $0.3 \text{ mM } \text{UO}_2^{2+}$

It can be seen that the first-order kinetics in the system without initially added UO_2^{2+} is not valid for the system with initially added UO_2^{2+} . The UO_2^{2+} dissolution rate is faster in the system with $10 \text{ mM } \text{HCO}_3^-$ followed by $5 \text{ mM } \text{HCO}_3^-$ and $2 \text{ mM } \text{HCO}_3^-$. There is decreasing trend in the system with $1 \text{ mM } \text{HCO}_3^-$; therefore, there is a UO_2^{2+} consumption in this system as discussed in Section 5.1.

Chapter 6

Conclusion

As a result of the experiments, it was concluded the UO_2^{2+} dissolution is found as higher in the system that has a higher HCO_3^- concentration because the HCO_3^- mitigates the accumulation of the dissolution products on the UO_2 surface. It was also found that oxidation of UO_2 is the rate limiting step at the beginning of the exposure. It was interpreted that the studdite is formed in the systems with 1 mM and 2 mM HCO_3^- with initially added UO_2^{2+} . The pH was found as increased mainly at the beginning of the exposure. No clear relationship was observed regarding the H_2O_2 species and dissolution mechanism; however, it was concluded that H_2O_2 speciation are more effective on the surface mechanism in the systems having lower HCO_3^- concentration. It was also observed that the H_2O_2 consumption kinetics is independent of HCO_3^- concentration. The UO_2^{2+} dissolution follows the first-order reaction kinetics with respect to HCO_3^- concentration in the system without initially added UO_2^{2+} . Finally, the rate of UO_2^{2+} dissolution decreases with the addition of UO_2^{2+} due to the species formed in the systems.

Acknowledgments

First of all, I would like to express my deepest appreciation to my supervisor Mats Jonsson for his endless patience, the time he allocates during his busiest period, his supportive and friendly attitude, and his constructive feedback. I am honored to work with you.

I would like to thank my colleagues Richard Härlin, Sawsan El Jamal, Junyi Li, Yi Yang for their friendship, scientific and emotional support. Thank you for trying to help me with my every question, even if it is not within your knowledge. Special thanks to Daniel Olsson for being ready in every moment during my experimental studies to teach me with endless patience. Thank you for finding answers to all my questions and analyzing my experimental results with me.

I also would like to thank all my teachers in the Nuclear Energy Engineering Department. Thank you for the knowledge you share with us. I am proud to work with you.

My deepest thanks to all my friends in Sweden, in Turkey, and all over the world. Thanks to your moral support, I was able to complete my education here. I would especially like to thank Dimitri Nikitopoulos and Georgios Zagoraios for making my life here easier. It would have been impossible for me to complete my education without your help.

In addition, I would like to express my sincere respect and thanks to Mr. Burak Gül, Stockholm Educational Counselor, who provided moral support for us. He cared for all our problems as if he were one of our family and made us feel that we were not alone here.

I would like to thank the Ministry of Higher Education of the Republic of Turkey for providing me with financial support that covers all my expenses during my master's study. It could have been challenging to pursue my dream without your support.

Last but not least, I would like to express my deepest gratitude to my family. My deepest thanks to you for being with me on this journey, getting stressed with me, and being happy with me, for your endless support, and for giving me peace with your presence. I could not have undertaken this journey without you. This is our success! Love you guys!

References

- [1] Michael J. Apted and Joonhong Ahn. 1 - repository 101: Multiple-barrier geological repository design and isolation strategies for safe disposal of radioactive materials. In Michael J. Apted and Joonhong Ahn, editors, *Geological Repository Systems for Safe Disposal of Spent Nuclear Fuels and Radioactive Waste (Second Edition)*, Woodhead Publishing Series in Energy, pages 3–26. Woodhead Publishing, second edition edition, 2017.
- [2] David W. Shoesmith. Fuel corrosion processes under waste disposal conditions. *Journal of Nuclear Materials*, 282(1):1–31, 2000.
- [3] Ella Ekeröth, Olivia Roth, and Mats Jonsson. The relative impact of radiolysis products in radiation induced oxidative dissolution of UO_2 . *Journal of Nuclear Materials*, 355(1):38–46, 2006.
- [4] John W.T. Spinks and R. J. Woods. *An introduction to radiation chemistry*. Wiley-Interscience, 1990.
- [5] Hilbert Christensen and Sham Sunder. Current state of knowledge of water radiolysis effects on spent nuclear fuel corrosion. *Nuclear Technology*, 131:102–123, 2000.
- [6] Catherine Corbel, Gaël Sattonnay, Séverine Guilbert, Frédéric Garrido, Marie France Barthe, and Christophe Jegou. Addition versus radiolytic production effects of hydrogen peroxide on aqueous corrosion of UO_2 . *Journal of Nuclear Materials*, 348(1):1–17, 2006.
- [7] Daniel Olsson, Junyi Li, and Mats Jonsson. Kinetic effects of H_2O_2 speciation on the overall peroxide consumption at UO_2 –water interfaces. *ACS Omega*, 7(18):15929–15935, 2022.
- [8] Annika Carolin Maier, Alexandre Barreiro Fidalgo, and Mats Jonsson. Impact of H_2 and consecutive H_2O_2 exposures on the oxidative dissolution of $\text{U}_{1-x}\text{Gd}_x\text{O}_2$ pellets under deep repository conditions for spent nuclear fuel. *European Journal of Inorganic Chemistry*, 2020(20):1946–1950, 2020.

-
- [9] Alexandre Barreiro Fidalgo, Björn Dahlgren, Tore Brinck, and Mats Jonsson. Surface reactions of H_2O_2 , H_2 , and O_2 in aqueous systems containing ZrO_2 . *The Journal of Physical Chemistry C*, 120(3):1609–1614, 2016.
- [10] Dong-Yong Chung, Min-Sung Park, Keun-Young Lee, Eil-Hee Lee, Kwang-Wook Kim, and Jei-Kwon Moon. Decomposition of uranyl peroxo-carbonato complex ion in the presence of metal oxides in carbonate media. *Journal of Radioanalytical and Nuclear Chemistry*, 306:761–768, 2015.
- [11] Sarah Hickam, Jaclyn Breier, Yasmeen Cripe, Erica Cole, and Peter C. Burns. Effects of H_2O_2 concentration on formation of uranyl peroxide species probed by dissolution of uranium nitride and uranium dioxide. *Inorganic Chemistry*, 58(9):5858–5864, 2019.
- [12] Kwang-Wook Kim, Jun-Taek Hyun, Keun-Young Lee, Eil-Hee Lee, Kune-Woo Lee, Kee-Chan Song, and Jei-Kwon Moon. Effects of the different conditions of uranyl and hydrogen peroxide solutions on the behavior of the uranium peroxide precipitation. *Journal of Hazardous Materials*, 193:52–58, 2011.
- [13] Frederic Clarens, Joan de Pablo, Ismael Díez-Pérez, Ignasi Casas, Javier Giménez, and Mireia Rovira. Formation of studtite during the oxidative dissolution of UO_2 by hydrogen peroxide: A SFM study. *Environmental science and technology*, 38(24):6656–6661, 2004.
- [14] Sara Sundin, Björn Dahlgren, Olivia Roth, and Mats Jonsson. H_2O_2 and radiation induced dissolution of UO_2 and simfuel in HCO_3^- deficient aqueous solution. *Journal of nuclear materials*, 443(1-3):291–297, 2013.
- [15] Ella Ekeröth and Mats Jonsson. Oxidation of UO_2 by radiolytic oxidants. *Journal of Nuclear Materials*, 322(2):242–248, 2003.
- [16] Mohammad Mohsin Hossain, Ella Ekeröth, and Mats Jonsson. Effects of HCO_3^- on the kinetics of UO_2 oxidation by H_2O_2 . *Journal of nuclear materials*, 358(2-3):202–208, 2006.
- [17] Junyi Li, Annika C. Maier, and Mats Jonsson. Stability of studtite in aqueous suspension: Impact of HCO_3^- and ionizing radiation on the dynamics of dissolution. *ACS Applied Energy Materials*, 3(1):352–357, 2020.
- [18] Jungjin Kim, HyunJu Kim, Won-Seok Kim, and Wooyong Um. Dissolution of studtite $[\text{UO}_2(\text{O}_2)(\text{H}_2\text{O})_4]$ in various geochemical conditions. *Journal of environmental radioactivity*, 189:57–66, 2018.

-
- [19] Junyi Li, Zoltán Szabó, and Mats Jonsson. Meta-studtite stability in aqueous solutions. impact of HCO_3^- , H_2O_2 and ionizing radiation on dissolution and speciation. *Dalton Trans.*, 50:6568–6577, 2021.
- [20] Ingmar Grenthe, Diego Ferri, Francesco Salvatore, and Guisepe Riccio. Studies on metal carbonate equilibria. Part 10. A solubility study of the complex formation in the uranium(VI)–water–carbon dioxide(g) system at 25°C. *J. Chem. Soc., Dalton Trans.*, pages 2439–2443, 1984.
- [21] Kwang-Wook Kim, Euo-Chang Jung, Keun-Young Lee, Hye-Ryun Cho, Eil-Hee Lee, and Dong-Yong Chung. Evaluation of the behavior of uranium peroxocarbonate complexes in $\text{Na} - \text{U(VI)} - \text{CO}_3 - \text{OH} - \text{H}_2\text{O}_2$ solutions by raman spectroscopy. *The Journal of Physical Chemistry A*, 116(49):12024–12031, 2012. PMID: 23181400.
- [22] Grace Lu, Tori Z. Forbes, and Amanda J. Haes. Evaluating best practices in raman spectral analysis for uranium speciation and relative abundance in aqueous solutions. *Analytical Chemistry*, 88(1):773–780, 2016. PMID: 26607279.
- [23] Kwang-Wook Kim, Keun-Young Lee, Dong-Yong Chung, Eil-Hee Lee, Jei-Kwon Moon, and Dong-Woo Shin. Evaluation of the stability of uranyl peroxocarbonato complex ions in carbonate media at different temperatures. *Journal of Hazardous Materials*, 233-234:213–218, 2012.
- [24] Chenxi Hou, Hui He, Jinjie Sun, Bei Yang, Haofan Fang, Caishan Jiao, and Mingjian He. Dissolution of uranium dioxide powder in carbonate-peroxide solution. *Journal of Radioanalytical and Nuclear Chemistry*, 331:2245–2252, 2022.
- [25] Christophe Jégou, Benoist Muzeau, Véronique Broudic, A. Poulesquen, Danièle Roudil, Frédéric Jorion, and Catherine Corbel. Effect of alpha irradiation on UO_2 surface reactivity in aqueous media. *Radiochimica Acta*, 93(1):35–42, 2005.
- [26] Mohammad Mohsin Hossain and Mats Jonsson. Effects of ionic strength on the kinetics for UO_2 oxidation. *Journal of Nuclear Materials*, 373(1):190–193, 2008.
- [27] Ghada El Jamal, Junyi Li, and Mats Jonsson. H_2O_2 -induced oxidative dissolution of UO_2 in saline solutions. *European Journal of Inorganic Chemistry*, 2021(40):4175–4182, 2021.
- [28] John R. Lamarsh. *Introduction to nuclear reactor theory*. Addison-Wesley series in nuclear engineering. Addison-Wesley Pub. Co., Reading, Mass, 1966.

-
- [29] E. Nihan Onder. 2-nuclear fuel. In Jovica R. Riznic, editor, *Pressurized Heavy Water Reactors*, volume 7 of *JSME Series in Thermal and Nuclear Power Generation*, pages 45–68. Elsevier, 2022.
- [30] International Atomic Energy Agency. Thermodynamic and transport properties of uranium dioxide and related phases. Technical Report 39, International Atomic Energy Agency, Vienna, 1965.
- [31] Jordi Bruno, Lara Duro, and François Diaz-Maurin. 13 - spent nuclear fuel and disposal. In Markus H.A. Piro, editor, *Advances in Nuclear Fuel Chemistry*, Woodhead Publishing Series in Energy, pages 527–553. Woodhead Publishing, 2020.
- [32] Jessica Veliscek-Carolan. Separation of actinides from spent nuclear fuel: A review. *Journal of Hazardous Materials*, 318:266–281, 2016.
- [33] Paul Carbol, Detlef H. Wegen, Thierry Wiss, Patrik Fors, Christophe Jegou, and Kastriot Spahiu. 6.13 - Spent Nuclear Fuel as Waste Material. In *Comprehensive Nuclear Materials (Second Edition)*, pages 347–386. Elsevier, Oxford, second edition edition, 2020.
- [34] Jean Radwan, J. Ly, and Delphine Hainos. New radiolysis-driven matrix dissolution operational model based on stationary UO_2 voltametric experiments. *Corrosion Science*, 199:110158, 2022.
- [35] Lena Morén, Roland Johansson, Karin Pers, and Marie Wiborgh. Design and production of the KBS-3 repository. Technical report, SKB, 2010.
- [36] Alexandre Barreiro Fidalgo and Mats Jonsson. Radiation induced dissolution of $(\text{U}, \text{Gd})\text{O}_2$ pellets in aqueous solution – A comparison to standard UO_2 pellets. *Journal of Nuclear Materials*, 514:216–223, 2019.
- [37] Kristina Nilsson, Olivia Roth, and Mats Jonsson. Oxidative dissolution of adopt compared to standard UO_2 fuel. *Journal of Nuclear Materials*, 488:123–128, 2017.
- [38] Sophie Le Caër. Water radiolysis: Influence of oxide surfaces on H_2 production under ionizing radiation. *Water*, 3(1):235–253, 2011.
- [39] David W. Shoesmith. Used Fuel And Uranium Dioxide Dissolution Studies - A Review Report No.: Nwmo-Tr-2007-03. Technical report, Corrosion 2008, New Orleans, Louisiana, 03 2008.
- [40] Mats Jonsson. Radiation effects on materials used in geological repositories for spent nuclear fuel. *ISRN materials science*, 2012:1–13, 2012.

-
- [41] Sham Sunder, David W. Shoemith, Hilbert Christensen, and Neil H. Miller. Oxidation of UO_2 fuel by the products of gamma radiolysis of water. *Journal of Nuclear Materials*, 190:78–86, 1992.
- [42] Thierry Mennecart, Bernd Grambow, M. Fattahi, and Z. Andriambololona. Effect of alpha radiolysis on doped UO_2 dissolution under reducing conditions. *Radiochimica Acta*, 92(9-11):611–615, 2004.
- [43] Frederick Sydney Dainton. The radiation chemistry of water and aqueous solutions. *Journal of the American Chemical Society*, 84(12):2467–2468, 1962.
- [44] Robert Guillaumont, Federico J Mompean, et al. *Update on the chemical thermodynamics of uranium, neptunium, plutonium, americium and technetium*, volume 5. Elsevier Amsterdam, 2003.
- [45] Alexandre Barreiro Fidalgo, Yuta Kumagai, and Mats Jonsson. The role of surface-bound hydroxyl radicals in the reaction between H_2O_2 and UO_2 . *Journal of Coordination Chemistry*, 71(11-13):1799–1807, 2018.
- [46] Sergey V. Krivovichev. 2.23 - Crystal chemistry of uranium oxides and minerals. In Jan Reedijk and Kenneth Poeppelmeier, editors, *Comprehensive Inorganic Chemistry II (Second Edition)*, pages 611–640. Elsevier, Amsterdam, second edition edition, 2013.
- [47] Shaun K. Frape, Andrew Blyth, Runar Blomqvist, Ralph H. McNutt, and Matthew Gascoyne. Deep fluids in the continents: II. crystalline rocks, 2004.
- [48] V.M. Oversby. Uranium dioxide, simfuel, and spent fuel dissolution rates - A review of published data (TR-99-22). Technical report, SKB, 1999.
- [49] Pier Luigi Zanonato, Plinio Di Bernardo, and Ingmar Grenthe. Chemical equilibria in the binary and ternary uranyl(VI)–hydroxide–peroxide systems. *Dalton Trans.*, 41:3380–3386, 2012.
- [50] Pier Luigi Zanonato, Plinio Di Bernardo, Zoltán Szabó, and Ingmar Grenthe. Chemical equilibria in the uranyl(VI)–peroxide–carbonate system; Identification of precursors for the formation of poly-peroxometallates. *Dalton Trans.*, 41:11635–11641, 2012.
- [51] Yuta Kumagai, Ryoji Kusaka, Masami Nakada, Masayuki Watanabe, Daisuke Akiyama, Akira Kirishima, Nobuaki Sato, and Takayuki Sasaki. Uranium dissolution and uranyl peroxide formation by immersion of simulated fuel debris in aqueous H_2O_2 solution. *Journal of Nuclear Science and Technology*, 0(0):1–11, 2022.

-
- [52] Mattias Olsson, Anna-Maria Jakobsson, and Yngve Albinsson. Surface charge densities of two actinide(IV) oxides: UO_2 and ThO_2 . *Journal of Colloid and Interface Science*, 256(2):256–261, 2002.
- [53] Ignasi Puigdomènech, Elisenda Colàs, Mireia Grivè, I Campos, and Diego García-Gil. A tool to draw chemical equilibrium diagrams using SIT: Applications to geochemical systems and radionuclide solubility. *MRS Online Proceedings Library*, 1665:111–116, 2014.
- [54] Jane E. Frew, Peter Jones, and George Scholes. Spectrophotometric determination of hydrogen peroxide and organic hydroperoxides at low concentrations in aqueous solution. *Analytica chimica acta*, 155:139–150, 1983.
- [55] Attgustine O Allen, C. J Hochanadel, J. A Ghormley, and T. W Davis. Decomposition of water and aqueous solutions under mixed fast neutron and γ -radiation. *Journal of physical chemistry (1952)*, 56(5):575–586, 1952.
- [56] Sergey B. Savvin. Analytical use of arsenazo iii: Determination of thorium, zirconium, uranium and rare earth elements. *Talanta (Oxford)*, 8(9):673–685, 1961.
- [57] Joan De Pablo, Ignasi Casas, Frederic Clarens, Fatima El Aamrani, and Miquel Rovira. The effect of hydrogen peroxide concentration on the oxidative dissolution of unirradiated uranium dioxide. *MRS proceedings*, 663, 2000.

Appendix

pH

Table 1: pH values measured during experiments in the system with 10 mM HCO_3^- , 0.2 mM H_2O_2 and 0.3 mM UO_2^{2+}

Time/ min	0	1290
pH	8.23	9.8

Table 2: pH values measured during experiments in the system with 10 mM HCO_3^- , 0.2 mM H_2O_2 without initially added UO_2^{2+}

Time/ min	0	420
pH	9	9.8

Table 3: pH values measured during experiments in the system with 5 mM HCO_3^- , 0.2 mM H_2O_2 and 0.3 mM UO_2^{2+}

Time/ min	1	14	47	120	240	1297
pH	7.1	8.2	9.2	9.6	9.6	10.3

Table 4: pH values measured during experiments in the system with 5 mM HCO_3^- , 0.2 mM H_2O_2 without initially added UO_2^{2+}

Time/ min	1	14	180
pH	8.5	8.8	9.5

Table 5: pH values measured during experiments in the system with 2 mM HCO_3^- , 0.2 mM H_2O_2 and 0.3 mM UO_2^{2+}

Time/ min	1	18	20	35	90	145	180	325	350
pH	6.7	8.25	8.1	8.1	9.1	9.2	9.2	9.6	9.6

Table 6: pH values measured during experiments in the system with 2 mM HCO_3^- , 0.2 mM H_2O_2 without initially added UO_2^{2+}

Time/ min	1	20	38	90	145	180	350
pH	8.6	9.1	9.2	9.2	9.3	9.3	9.5

Table 7: pH values measured during experiments in the system with 1 mM HCO_3^- , 0.2 mM H_2O_2 and 0.3 mM UO_2^{2+}

Time/ min	1	30	85	150	330	435	1320	1440	1620	2820
pH	6.4	7.5	7.8	8.1	8.2	8.9	9.2	9	9.2	9.3

Table 8: pH values measured during experiments in the system with 1 mM HCO_3^- , 0.2 mM H_2O_2 without initially added UO_2^{2+}

Time/ min	1	35	85	330	435	1320	1440	1620	2820
ph	8.5	8.9	8.6	9	9.5	9.5	9.7	9.8	9.6

Speciation Calculation

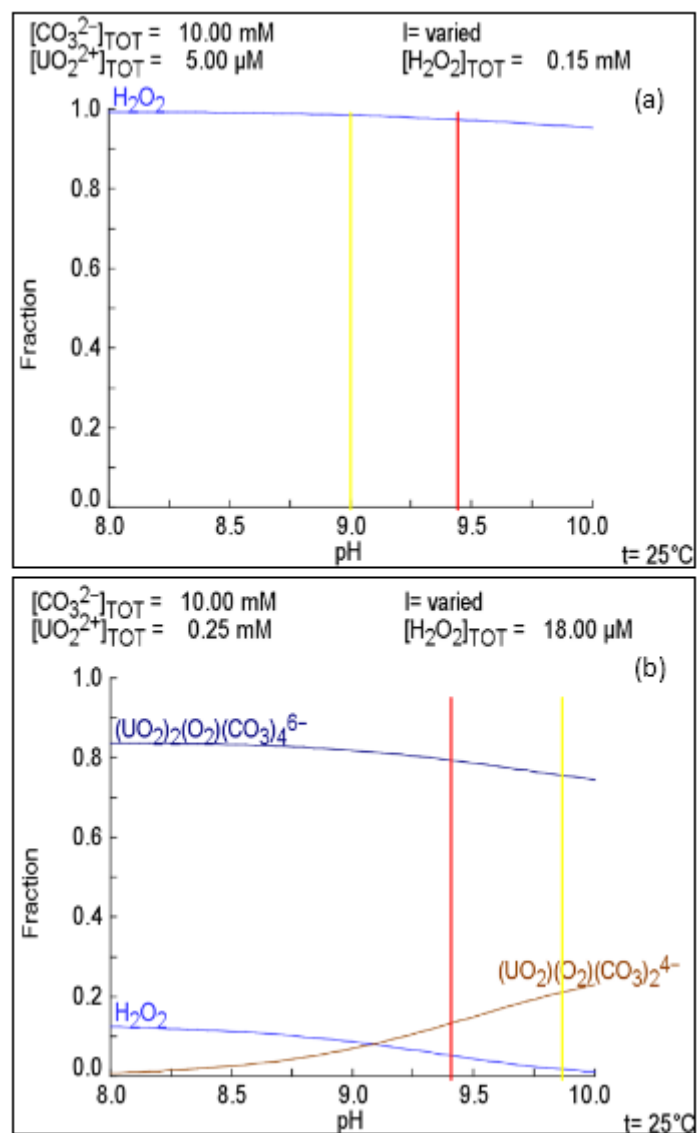


Figure 1: Speciation calculation prepared in SPANA with the data at (a) 0.5 min and (b) 420 min of exposure for the system with 10 mM HCO_3^- , 0.2 mM H_2O_2 without initially added UO_2^{2+}

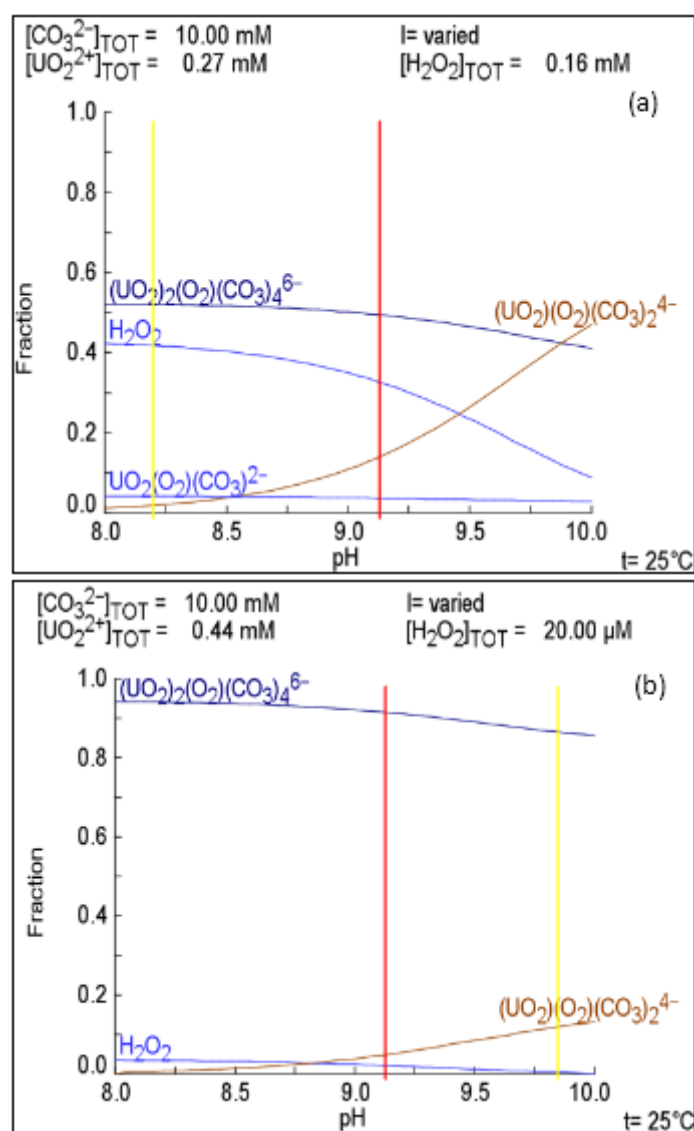


Figure 2: Speciation calculation prepared in SPANA with the data at (a) 0.5 min and (b) 300 min of exposure for the system with 10 mM HCO_3^- , 0.2 mM H_2O_2 with initially added 0.3 mM UO_2^{2+}

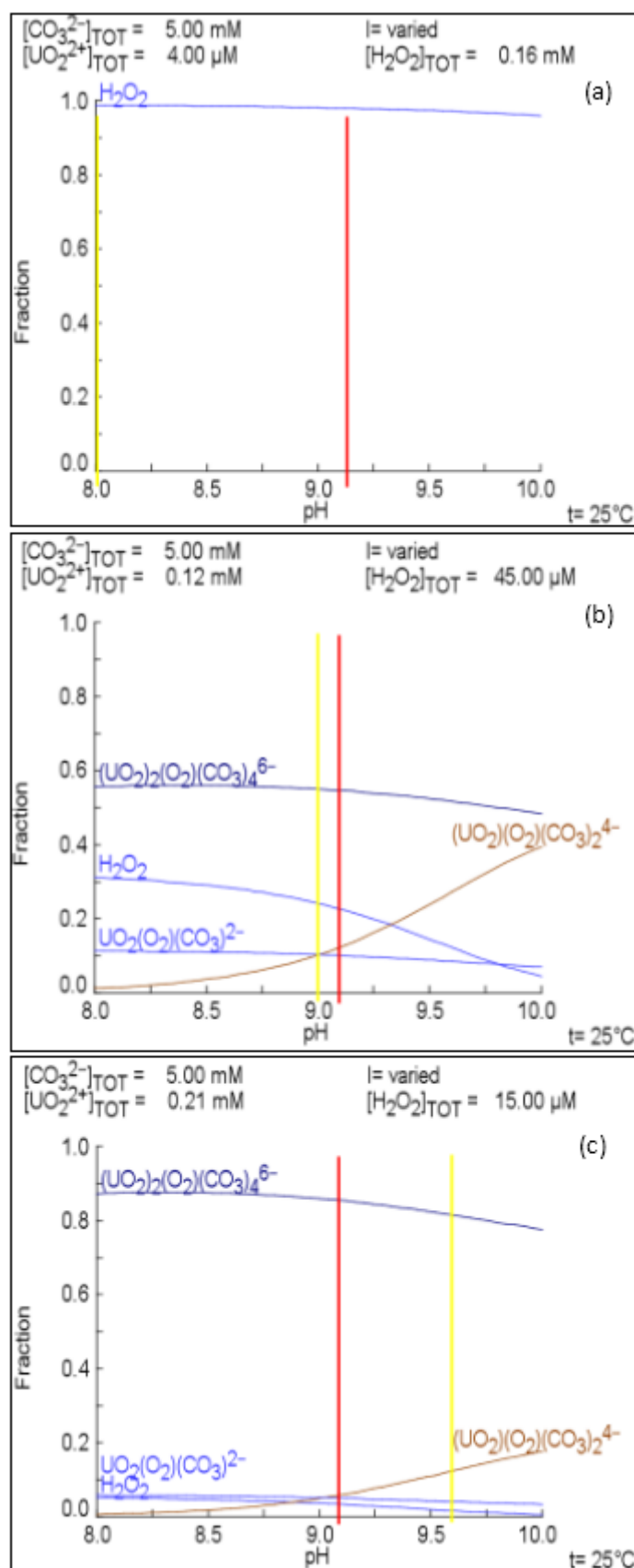


Figure 3: Speciation calculation prepared in SPANA with the data at (a) 0.5 min, (b) 60 min and (c) 300 min of exposure for the system with 5 mM HCO_3^- , 0.2 mM H_2O_2 without initially added UO_2^{2+}

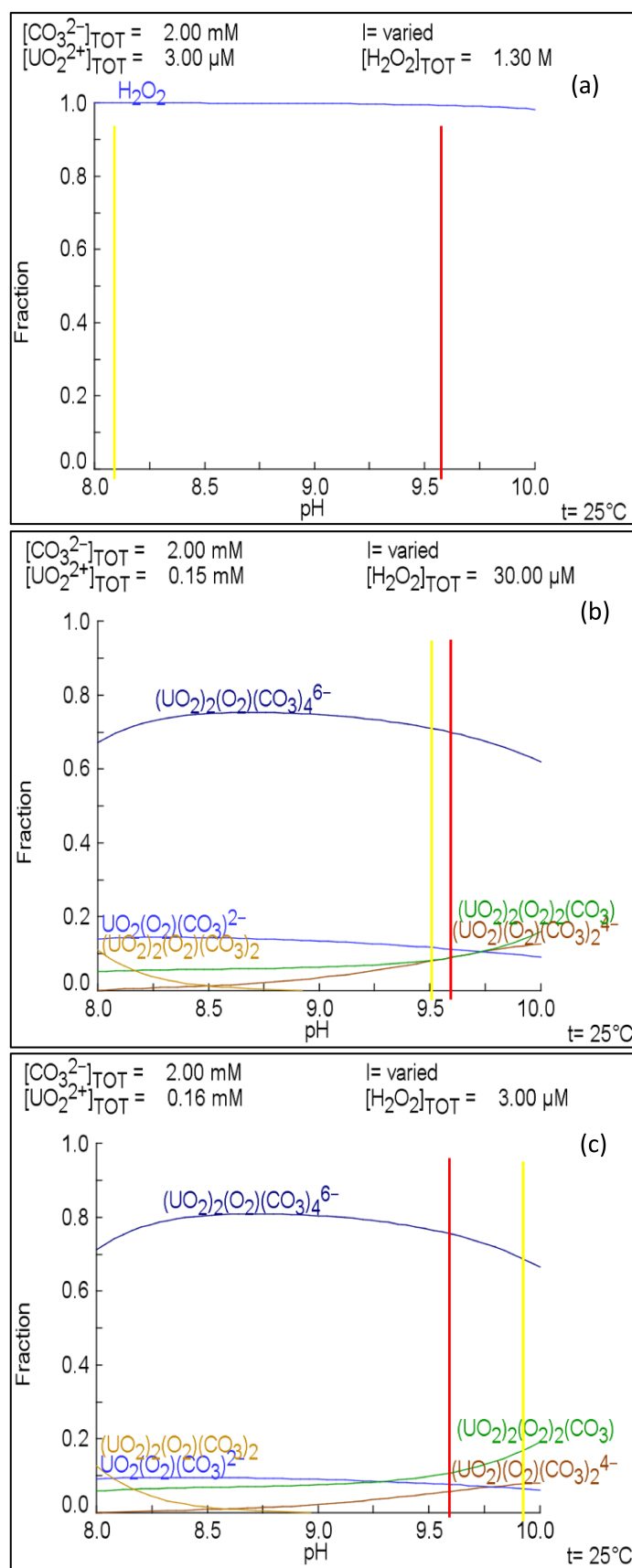


Figure 4: Speciation calculation prepared in SPANA with the data at (a) 0.5 min, (b) 60 min and (c) 300 min of exposure for the system with 2 mM HCO_3^- , 0.2 mM H_2O_2 without initially added UO_2^{2+}

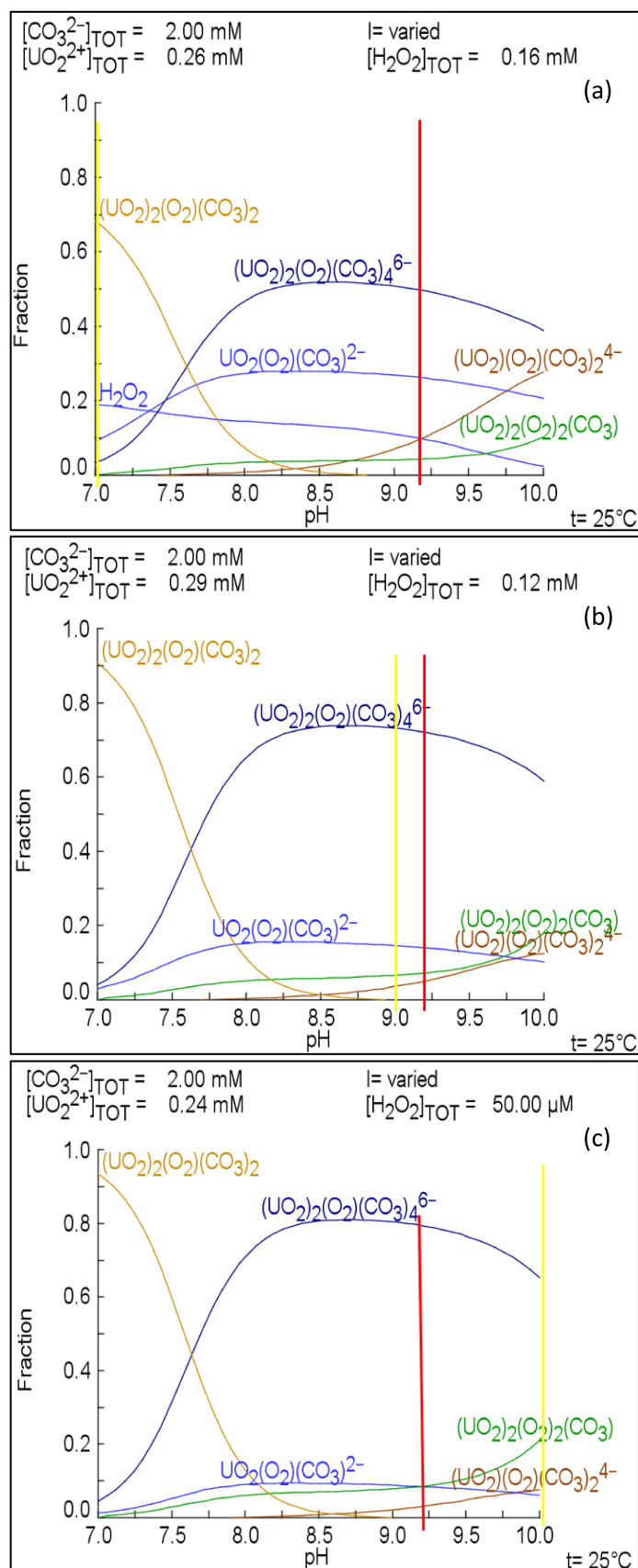


Figure 5: Speciation calculation prepared in SPANA with the data at (a) 0.5 min, (b) 60 min and (c) 300 min of exposure for the system with 2 mM HCO_3^- , 0.2 mM H_2O_2 with initially added UO_2^{2+}

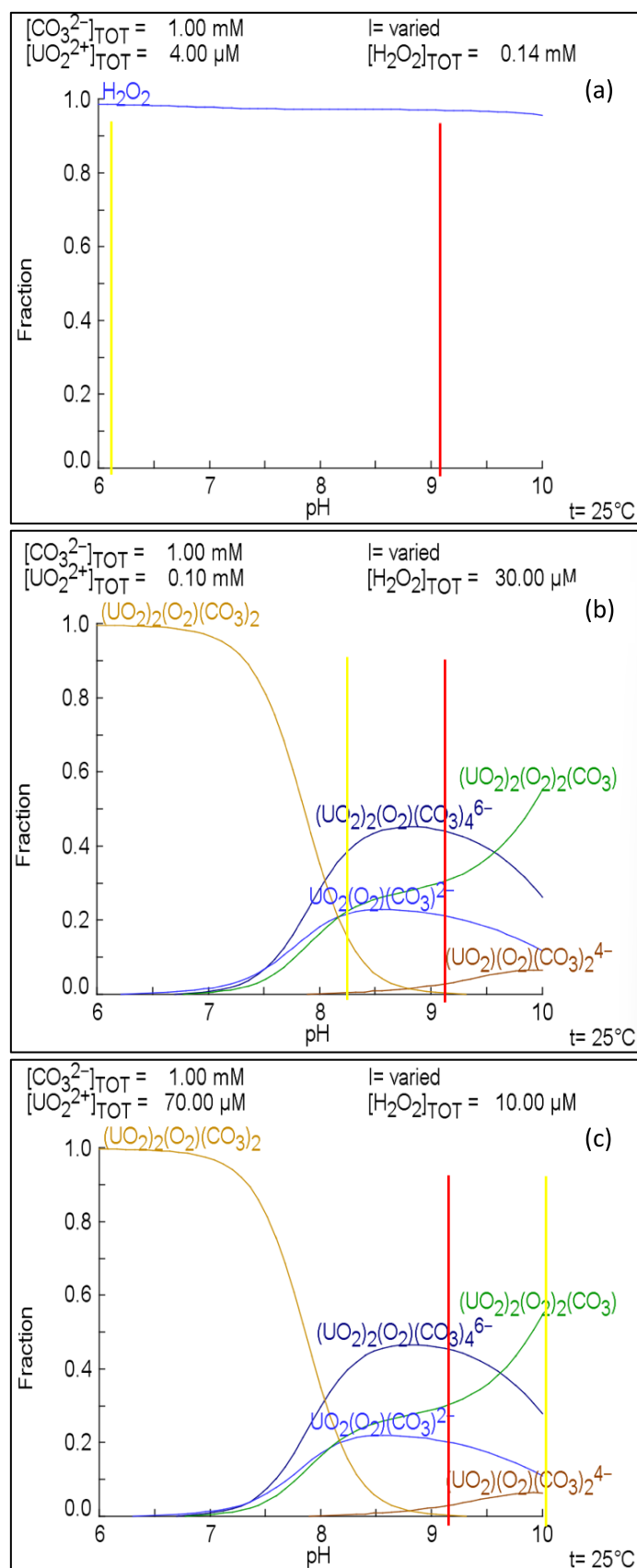


Figure 6: Speciation calculation prepared in SPANA with the data at (a) 0.5 min, (b) 60 min and (c) 300 min of exposure for the system with 1 mM HCO_3^- , 0.2 mM H_2O_2 without initially added UO_2^{2+}

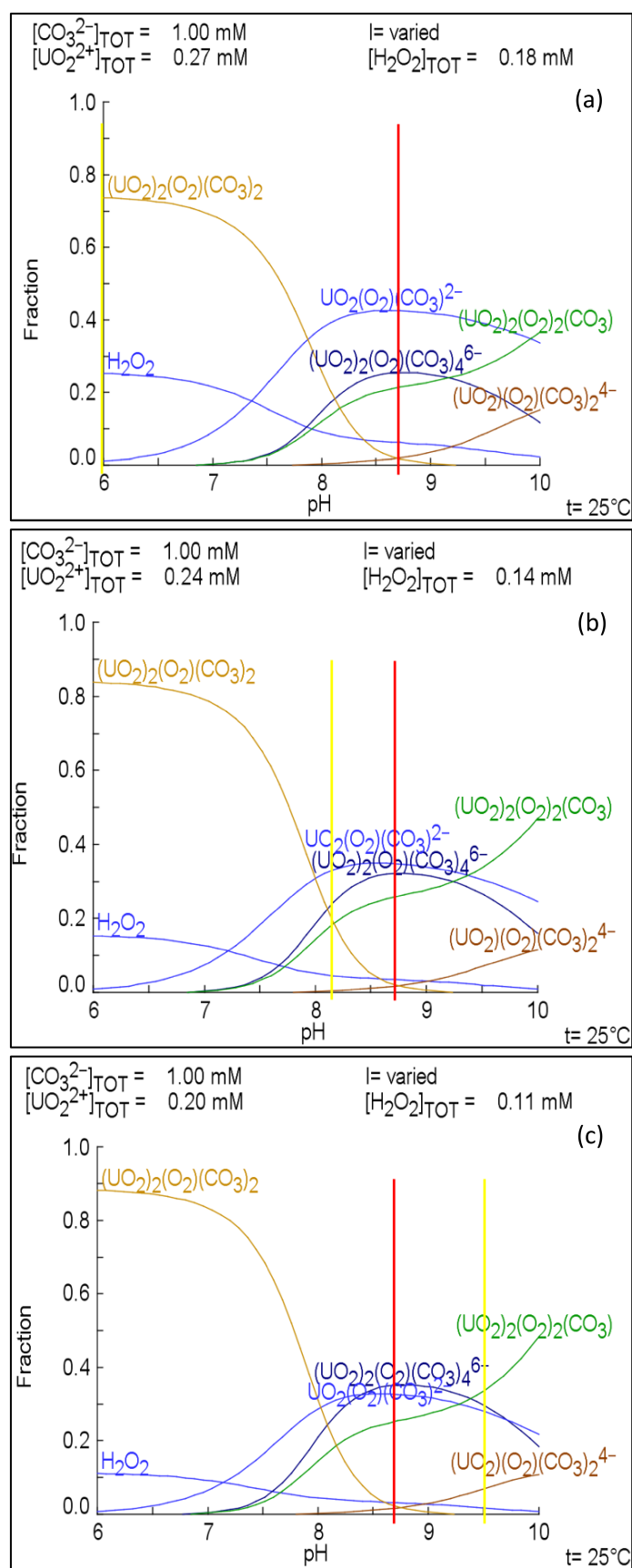


Figure 7: Speciation calculation prepared in SPANA with the data at (a) 0.5 min, (b) 60 min and (c) 300 min of exposure for the system with 1 mM HCO_3^- , $0.2 \text{ mM H}_2\text{O}_2$ with initially added UO_2^{2+}